Journal of Thermal Analysis and Calorimetry (2025) 150:10549–10573
https://doi.org/10.1007/s10973-025-14399-y

Experimental investigation and machine learning modeling of the effects of hybridization mixing ratio, nanoparticle type, and temperature on the thermophysical properties of Fe_3O_4/TiO_2, Fe_3O_4/MgO, and Fe_3O_4/ZnO-DI water hybrid ferrofluids

Victor O. Adogbeji[1] · Emmanuel O. Atofarati[2] · Mohsen Sharifpur[1,3,4] · Josua P. Meyer[5]

Received: 23 July 2024 / Accepted: 8 May 2025 / Published online: 14 June 2025

Abstract

This study experimentally investigates the influence of hybridization mixing ratio (HMR), nanoparticle size, and temperature on the stability, thermal conductivity, viscosity, and thermoelectric conductivity of Fe_3O_4/TiO_2-DIW, Fe_3O_4/MgO-DIW, and Fe_3O_4/ZnO-DIW magnetic hybrid ferrofluids (MHFs). A two-step preparation technique was used to synthesize 0.3% volume concentration of the MHFs at HMRs of 80:20, 60:40, and 40:60, respectively. The study's result revealed that the thermal and electrical conductivity of the MHF was proportional to the temperature of the MHF. Also, the viscosity and thermoelectric conductivity (TEC) of the MHF was inversely related to the MHF's temperature. The (80:20) ratio consistently stands out for superior stability and thermal conductivity. An exceptional electrical conductivity of 4.23 mS/cm was displayed by the Fe_3O_4/TiO_2(18 nm)-DIW at 50 °C. The best thermal conductivity–viscosity balance was observed for the Fe_3O_4/ZnO-DIW with HMR of 80:20 at 50 °C as it has the highest thermal conductivity enhancement of 31.28% and the least viscosity. These findings guide MHF customization, emphasizing stability and thermophysical performance balance. Fe_3O_4/ZnO-DI also had the best TEC value, making it most suitable for cooling PEM fuel cells. Linear regression analysis was used to generate the thermal conductivity correlations for the MHFs, while feature importance analysis highlights temperature as the most significant variable influencing their thermal conductivity.

Keywords Magnetic hybrid ferrofluids (MHFs) · Stability · Hybridization mixing ratios · Viscosity · Thermal conductivity · Heat transfer efficiency

✉ Victor O. Adogbeji
adogbeji.victor@mapoly.edu.ng

✉ Mohsen Sharifpur
mohsen.sharifpur@up.ac.za

[1] Department of Mechanical and Aeronautical Engineering, University of Pretoria, Private Bag X20, Pretoria, Hatfield 0028, South Africa

[2] Department of Mechanical and Bioresource and Biomedical Engineering, University of South Africa, Science Campus, Johannesburg, Florida 1710, South Africa

[3] School of Mechanical, Industrial and Aeronautical Engineering, University of the Witwatersrand, Wits, Private Bag 3, Johannesburg 2050, South Africa

[4] Department of Medical Research, China Medical University, Taichung, Taiwan

[5] Department of Mechanical and Mechatronic Engineering, Stellenbosch University, Stellenbosch, South Africa

Abbreviations

After Prep	Immediately after preparation
Ag	Silver nanoparticles
Al	Aluminum nanoparticles
AL_2O_3	Aluminum oxide nanoparticles
Au	Gold nanoparticles
Co_2O_3	Cobalt (III) oxide nanoparticles
Cu	Copper nanoparticles
CuO	Copper oxide nanoparticles
CNTs	Carbon nanotubes
DIW	Deionized water
DW	Distilled water
EG	Ethylene glycol
Fe_2O_3	Iron (III) oxide nanoparticles
Fe_3O_4	Iron (IV) oxide nanoparticles
GA	Gum arabic
GNP	Graphene nanoplatelets
GO	Graphene oxide
IEP	Isoelectric point

MgO	Magnesium oxide nanoparticles
MHNFs	Magnetic hybrid nanofluids
MHFs	Magnetic hybrid ferrofluids
MNPs	Magnetic nanoparticles
MWCNT	Multiwalled carbon nanoparticle
ND	Nanodiamond
Ni	Nickel nanoparticles
SF	Sedimentation factor
CV	Cross-validation
R	Residuals
MAE	Means average error
MSE	Mean square error
SiO_2	Silicon oxide nanoparticles
STDEV	Standard deviation
TEC	Thermoelectric conductivity
TEM	Transmission electron microscopy
Ti O_2	Titanium oxide nanoparticles
ZnO	Zinc oxide nanoparticles
UV–Vis	Ultraviolet–visible
X-NP	Defined nanoparticle

Greek symbols

Φ	Volume concentration (vol%)
μ	Viscosity (mPas)
κ	Thermal conductivity (Wm/K^{-1})
σ	Electrical conductivity (mS/cm^{-1})
ρ	Density (gcm^{-3})

Subscripts

A_0	Initial absorbance
A_t	Final absorbance

Introduction

More efficient ways to enhance heat transfer are imperative to pursue sustainable energy in various industrial and energy devices. One of the novel approaches to enhance the thermal performance of existing designs in various thermal devices is to adopt a novel heat transfer fluid called nanofluids. The concept of nanofluid was originally introduced in the work of Choi and Eastman [1]. In the study, they proposed that incorporating nanoparticles into conventional base fluids could enhance the fluid's thermal conductivity.

Subsequently, several experimental studies have been conducted to explore different types of nanoparticles (NPs) used in nanofluid research. These include metallic NPs, non-metallic oxide NPs, metallic oxide NPs, metallic carbide NPs, metallic nitride NPs, carbon-based NPs, etc., which could be magnetic or non-magnetic. Several studies have examined the influence of factors such as volume fraction, particle size, temperature, concentration, and other parameters on the thermal conductivity of the nanofluid. Their findings correspond with Choi and Eastman's proposition that nanofluids yield a significant enhancement in thermal conductivity compared to base fluids [2–4].

Magnetic nanoparticles (MNPs) are special ferromagnetic nanoparticles with a particle size below 100 nm. Common MNPs studied in the nanofluid field are magnetite (Fe_3O_4), maghemite (γ-Fe_3O_4), cobalt (Co_2O_3), hematite (Fe_2O_3), and nickel (Ni). These nanoparticles can be manipulated and effectively controlled in a magnetic field. However, magnetite (Fe_3O_4) possesses the most influential properties compared to other magnetic nanoparticles due to its inverse spinel structure, because the Fe^{3+} ion is available at both the octahedral and tetrahedral crystallization sites [5].

Ferrofluids, also called magnetic nanofluids (MNFs), are engineered by dispersing ferromagnetic nanoparticles in a conventional heat transfer fluid. Extensive research is currently being conducted on the use of MNFs, since the presence of MNPs improves the thermal properties of nanofluids and offers more outstanding properties due to their magnetic nature [6]. MNFs are usually prepared with a base fluid such as water, polar liquids, i.e., they are miscible with water (e.g., propylene glycol and ethylene glycol), or non-polar liquids, which are immiscible with water (e.g., kerosene, transformer oil, and motor oil) [6–9].

While a significant improvement in thermal conductivity was observed with single nanoparticle nanofluids, challenges related to stability remain. Additionally, the increased viscosity is recognized as a considerable drawback [10]. According to Chakraborty et al. [11], unstable nanofluids compromise nanofluid performance as the particle clustering and settling raise viscosity and undermine thermal properties, escalating costs [12], ineffectiveness for medical uses [13], and reduced oil recovery in petrochemical industries [14]. The particle clustering and settling raise viscosity and undermine thermal properties, escalating costs.

These, among other reasons, led to the hybridization of nanoparticles with higher stability potential, 'MNPs,' to enhance their stability while improving the thermal conductivity for optimized performance of nanofluids as heat transfer fluid with controlled magnetic response or specific functional characteristics, depending on their intended application.

Jana and colleagues [15] pioneered hybrid nanofluid research, aiming to enhance thermal conductivity and stability. They synthesized the hybrid nanofluids with carbon nanotubes-copper nanoparticles (CNTs-Cu) and carbon nanotubes-gold nanoparticles (CNTs-Au). Surprisingly, the hybrid nanofluids showed reduced thermal conductivity compared to single nanoparticle nanofluids. Giwa et al. [16] prepared AL_2O_3/MWCNT-Water nanofluid and observed a 14.17% increase in thermal conductivity value compared to individual nanofluid.

Chinnasamy et al. [17] formulated Fe_3O_4/MWCNT-Water nanofluid, and it was found that the thermal conductivity

of this nanofluid increased by 6.3% in comparison with pure Fe_3O_4 and MWCNT with high dispersion stability at a zeta potential of −40 mV. Harandi et al. [18] explored the impact of volume concentration and temperature on the thermal conductivity of EG-based hybrid nanofluids comprising functionalized Fe_3O_4/MWCNT (with equal volumes). Results showed a 30% increase at 50 °C and 2.3% volume concentration. Sundar et al. [19] synthesized nanodiamond/Fe_3O_4 observed a maximum enhancement of 17.8% compared to individual nanofluid. Mehrali et al. [20] hybridized graphene/Fe_3O_4 and observed 11% enhancement of the thermal conductivity. Acharya and Mabood [21] conducted a mathematical analysis of the hydrothermal behavior of graphene/Fe_3O_4-Water as a radiative heat transfer fluid. Their study revealed that higher heat transfer rates are associated with increased nanosuspension concentration, corresponding to improved thermal conductivity. In a similar vein, Lund et al. [22] investigated the viscous dissipation of Cu/Fe_3O_4 -Water nanofluid under the influence of a magnetic field, employing mathematical modeling to understand the fluid dynamics and heat transfer mechanisms in such systems.

Areum et al. [23] prepared Fe_3O_4/MWCNT/Water-ethylene glycol (80:20)-based nanofluid and reported a 2% enhancement in thermal conductivity, along with a stable nanofluid, as indicated by zeta potential measurements within the range of −32 to −56 mV over one month. Giwa et al. [24] conducted a study of hybridized MWCNT-Fe_2O_3 /DIW nanofluids, resulting in stable mixtures. They found that increasing volume concentration raised electrical conductivity and viscosity. However, with rising temperature, viscosity decreased, while electrical conductivity increased. These hybrid nanofluids showed substantial improvements in both properties compared to the base fluid, with viscosity increasing up to 35.7% improvement in thermal conductivity and electrical conductivity enhancement of up to 1676.4%. Sundar et al. [25] demonstrated the thermal conductivity of nanofluids containing 0.3 mass% of Fe_3O_4/MWCNT/Water. They observed that the thermal conductivity was significantly enhanced by showing an improvement of 13.88–28.46% in the hybrid at 0.3%, relative to the base fluid with a temperature range of 25–60 °C. Shi et al. [26] conducted a study to examine the thermophysical properties, namely viscosity, thermal conductivity, and specific heat capacity, of Fe_3O_4 nanofluid and Fe_3O_4/MWCNT/Water nanofluid at a concentration of 0.25 vol%. Their research outputs show that the hybrid nanofluid exhibited higher thermal conductivity and viscosity while demonstrating a lower specific heat capacity compared to the Fe_3O_4 nanofluid.

Several other studies focused on the thermal conductivity of magnetic hybrid nanofluid under the influence of magnetic fields and observed a significant enhancement. Shahsavar et al. [27] demonstrated that the thermal conductivity of nanofluids containing Fe_3O_4/CNT-Water at a ratio of (1:2, 2:1, and 1:1) under the magnetic field effect with the maximum enhancement of 12.07%,152.95%, and 141.80%, respectively, with a magnetic strength of 470mT. Liu et al.[28] prepared Fe_3O_4/CNT-Water with the effect of oscillating and a constant magnetic field of 700 Gauss, and they observed an enhancement of 22.62 and 24.25%, respectively, and reported that the nanofluid was stable and the thermal conductivity data were reproducible over a period of one month with zeta potential more than 40 and 60 mV. Korel et al. [29] examined the effects of a magnetic field on heat and fluid flow under mixed convection in an arc-shaped, lid-driven cavity filled with Fe_3O_4/water ferrofluid. Using a custom finite volume solver in Open FOAM®, they analyzed the influence of magnetic number (Mn), Richardson number (Ri), nanoparticle concentration (φ), and arc width ratio (b*/L). Results showed that applying the magnetic field near the heat source induced recirculation zones, enhancing thermal diffusion. At Ri = 0.04, heat transfer improved by up to 338.35% due to the combined effects of magnetism, curved walls, and nanoparticles. However, at Ri = 40, the presence of the Kelvin force led to a reduction in heat transfer. Two new Nusselt number correlations were also proposed based on the investigated parameters.

Baby and Sundara [30] introduced a magnetic nanofluid by dispersing silicon dioxide-coated Fe_3O_4 particle-decorated CNTs (Fe_3O_4 + SiO_2/CNT) in DIW. Their results indicated water-based nanofluids containing Fe_3O_4/CNTs and Fe_3O_4/SiO_2. When subjected to a magnetic field, CNT exhibited thermal conductivity enhancements of 20% and 24.5%, respectively, at a volume concentration of 0.03%.

Additionally, the integration of machine learning (ML) models for the prediction and optimization of nanofluid properties has been increasingly explored, Riyadi et al. [31]. Recent studies have shown the potential of artificial neural networks (ANNs) [32] and support vector machines (SVM) [33] in predicting thermophysical properties of nanofluids based on input variables such as nanoparticle type, size, and concentration, Zhang et al. [34]. These ML techniques can provide rapid and accurate predictions, reducing the need for extensive experimental work and facilitating the design of nanofluids with tailored properties for specific applications.

An extensive review of previous research reveals a predominant focus on two types of nanoparticles: MWCNT and CNT with MNPs for magnetic hybrid ferrofluids (MHFs). However, a substantial research gap exists regarding the stability and thermophysical properties of hybrid ferrofluids of Fe_3O_4 and other types of nanoparticles (TiO_2, MgO, ZnO, Au, Ag, etc.) other than carbon NPs. Also, the prevalent use of the hybridization mixing ratio (Fe_3O_4: X-NP; 80:20) in most studies poses a question to this author. Therefore, further investigation is crucial to elucidate the rationale behind the 80:20 Fe_3O_4 ratio and explore the influence of

hybridization on diverse hybrid ferrofluids for enhanced heat transfer applications.

This study aims to address this gap by experimentally investigating the stability, thermal conductivity, viscosity, electrical conductivity, and pH of Fe_3O_4/TiO_2-DIW, Fe_3O_4 /MgO-DIW, and Fe_3O_4/ZnO-DIW hybrid ferrofluids. The investigation involves a fixed volume concentration of 0.3%, hybridization mixing ratios of 80:20, 60:40, and 40:60 (mass percent basis), and thermophysical properties evaluated from 10 °C to 50 °C. To broaden the applications of magnetic nanofluids, this study explores hybridizing different nanoparticles with various mixing ratios, therefore addressing a major gap in the field of magnetic hybrid ferrofluids (MHFs) stability and thermophysical properties, which will further broaden their potential applications.

Materials and methodology

Materials

The magnetic nanoparticles consisted of iron (III) oxide, Fe_3O_4, with a particle size ranging from 20 to 30 nm and a purity of 95.5%. Titanium dioxide (TiO_2) was used in two variants, with particle sizes of 18 nm and 60 nm and purity levels of 99.9% and 99.8%, respectively. Magnesium oxide (MgO), with a particle size of 20 nm and a purity of 99.9%, and zinc oxide (ZnO), with a particle size of 20 nm and a purity of 99.5%, were also utilized. The respective manufacturers provided the specified nanoparticle diameters. The 60-nm particles of ZnO and TiO_2 were sourced from Nanostructured and Amorphous Materials Inc. in Houston, Texas, USA, while the others were procured from US Research Nanomaterial Inc. in Houston, Texas, USA. Gum arabic (GA) with a purity of $\geq$ 98.5%, obtained from Sigma-Aldrich in Berlin, Germany, was used as a surfactant to enhance the stability of the magnetic hybrid nanofluids. Table 1 presents the thermal properties of both the base fluid and nanoparticles used in this study. Note that some properties and parameters of the nanomaterials were sourced from the product datasheets provided by the respective companies.

Description of experimental procedures

The preparation of MHFs involved suspending nanoparticles in deionized water (DIW) and was carried out using a (Qsonica Q-700) ultrasonicator. The ultrasonication process lasted for 4 h, with a programmed sequence of 5-s pulses followed by 2-s intervals to ensure effective stability. To maintain the desired temperature during sonication and while assessing thermophysical characteristics, we used a programmable water bath (LAUDA ECO RE1225, Berlin, Germany) to ensure precise temperature control.

Throughout the study, various pieces of equipment were employed for different purposes. These included a digital weighing balance (Radwag AS 220.R2, Radom, Poland) with an accuracy of $\pm$ 0.01 g, a pH meter (Jenway 3510, Staffordshire, UK) with a range of -2 to 19.999 and an accuracy of $\pm$ 0.003, a vibro-viscometer (SV-10A series, A&D, Tokyo, Japan) with an accuracy of $\pm$ 1%, a UV–Visible spectrophotometer (Jenway, Staffordshire, UK), a transmission electron microscope (JEOL JEM-2100F, Tokyo, Japan) used for analyzing dry samples, and a conductivity meter (CHAUVIN ARNOUX, C.A 10141 Instrument, France) with an accuracy of $\pm$ 1%. These instruments served various purposes during the research, enabling comprehensive analysis and reliable measurements.

Furthermore, the prepared MHFs were characterized for thermal conductivity (K) and viscosity (μ) at different temperatures ranging from 10 to 50 °C using a KD2 pro (Decagon Devices Inc.) Thermal Properties Analyzer (METER Group) with an accuracy of $\pm$ 10% for K in the range of 0.02–2.0 W/m/K. This allowed for an assessment of the thermal properties of the MHFs at varying temperatures. Utilizing these techniques and instruments, we comprehensively evaluated the stability, thermophysical properties, and other characteristics of the MHFs, ensuring accurate and reliable results.

Magnetic hybrid nanofluid preparation and characterization

The preparation of hybrid nanofluids (MHFs) involved a two-step method, where varying proportions of Fe_3O_4 were

Table 1 Thermophysical properties of the nanoparticles at room temperature (25 °C)

Properties	Deionized water	Fe_3O_4	TiO_2		MgO	ZnO
			18 nm	60 nm		
Density/ kg m^{-3}	997	4950	4175	4230	3580	100–200
Thermal conductivity/ W m^{-1} K^{-1}	0.613	80.4	8.4	8.4	54.9	29
Specific heat capacity/ J $kg^{-1}.K^{-1}$	4179	670	692	–	–	–
Shape	–	Plate-like nanosheet	Spherical	Spherical	Spherical	Spherical

combined with TiO_2, MgO, and ZnO, constituting 80%, 60%, and 40% for Fe_3O_4, and 20%, 40%, and 60% for TiO_2, MgO, and ZnO, respectively. To ensure MHF stability, we rigorously monitored specific parameters, including thermal conductivity, viscosity, electrical conductivity, and pH over a temperature range of 5–50 °C. This monitoring began immediately after sonication and continued at varying temperature settings for one week. A follow-up assessment was carried out a month later using the same temperature range of 5–50 °C. During the sonication process, uniform conditions were maintained for all MHFs. All MHFs were maintained at a 0.3% volume concentration and 20 °C. The sonication parameters, which included an amplitude of 100, a frequency of 2 Hz, and a sonication time of 4-h, remained the same for all MHFs.

In this formulation, gum arabic served as the surfactant with mass ratios of 0.75% for TiO_2 and 0.5% for MgO and ZnO, contributing to the stabilization of the MHFs. The MHFs with a volume concentration of 0.3% were prepared following Eq. (1) [24, 35].

$$\Phi = \left(\frac{Y_{Fe_3O_4}\left(\frac{W}{\rho}\right)_{Fe_3O_4} + Y_X\left(\frac{W}{\rho}\right)_X}{Y_{Fe_3O_4}\left(\frac{W}{\rho}\right)_{Fe_3O_4} + Y_X\left(\frac{W}{\rho}\right)_X + \left(\frac{W}{\rho}\right)_{DIW}} \right) \quad (1)$$

where Y represents the proportion of each nanoparticle type, and X being TiO_2, MgO and ZnO particles, respectively.

The morphology and dispersion of MHFs were examined through transmission electron microscopy (TEM). The overall stability of the nanofluid, meaning that at least one of the measured properties (such as viscosity, UV–visible spectrophotometry, or thermal conductivity), should remain consistent, either for each individual measurement or across the overall assessment period, to indicate stability. This ensures that the nanofluid does not experience significant changes in its characteristics during the assessment. Our study conducted comprehensive analyses were performed immediately after sonication and one month later, under the same conditions at temperatures from 10 to 50 °C. Weekly visual inspections were conducted for a month. By utilizing this multifaceted approach, we thoroughly evaluated the MHFs' stability, considering their morphology, dispersion, optical properties, surface charge, thermal properties, and visual appearance.

Measurement of thermal conductivity setup

The experimental setup included a constant temperature bath (LAUDA ECO RE1225) for precise temperature control during thermal conductivity measurements. Measurements were taken over 24 h and 15 min at temperatures from 10 to 50 °C with 5 °C intervals. After one month, the measurements were repeated. The KD2 Pro from Decagon Devices Inc., with an operating range of 0.02–2 W m^{-1} K^{-1} and 5% uncertainty, was employed. It utilized a single-needle sensor (1.3 mm diameter, 60 mm length) and the transient hot-wire method for thermal conductivity measurement.

Viscosity measurement

Viscosity measurements are essential for evaluating nanofluid stability. In this study, viscosity assessments for MHFs (Fe_3O_4/TiO_2/DIW, Fe_3O_4/MgO/DIW, and Fe_3O_4/ZnO/DIW) were conducted at temperatures between 10 °C and 50 °C. Prior to the measurements, the vibro-viscometer was calibrated to ensure accuracy. A programmable water bath (LAUDA, Berlin, Germany, model ECO RE1225) maintained a consistent temperature. Initial viscosity measurements were taken immediately after nanofluid preparation and monitored for 24 h and 15 min. These measurements, conducted under varying temperatures and time intervals, provided crucial insights into nanofluid stability, facilitating a comprehensive understanding of their behavior over time and in different thermal conditions.

Measurement of electrical conductivity and pH

A standard calibration fluid supplied by the manufacturer was used to calibrate the electrical conductivity meter. The calibration involved measuring the standard fluid at 25°C in triplicates, and the average electrical conductivity was recorded as 1413.6 μS·cm**1**. Subsequently, the electrical conductivity of the MHFs nanofluids was determined at temperatures ranging from 10 to 50 °C, with 5 °C intervals. The pH meter was calibrated using buffer solutions with pH values of 4, 7, and 10. The pH values of the MHFs nanofluids were measured at temperatures varying from 10°C to 50°C, with 5°C intervals, with an uncertainty of 0.04% compared to DIW.

UV–Vis spectroscopy for estimating relative stability

Ultraviolet–visible (UV–Vis) spectroscopy quantitatively assessed the stability of MHFs (Fe_3O_4/TiO_2-DIW, Fe_3O_4/MgO-DIW, and Fe_3O_4/ZnO-DIW) nanofluid samples. The Beer-Lambert law ($A = \alpha LC$) was employed, establishing a linear relationship between light absorbance and material properties. Absorbance (A) depended on the absorption coefficient (α), light path length (L), and substance concentration (C) as per Beer-Lambert law. After preparation, MHFs were analyzed in a UV–Vis spectrometer (ONDA TOUCH UV-21 Spectrophotometer, 4nm bandwidth) at room temperature. DIW was used for calibration, and all results were repeated six times for accuracy. The absorbance was measured at different wavelengths ranging from

200 to 300 nm, with intervals of 10 nm from 200 to 280 nm and intervals of 1 nm from 281 to 300 nm for all samples. Standard graphs were created for each MHFs, facilitating relative stability comparisons based on absorbance values. The following procedure was employed to determine the percentage of sedimentation in various (MHFs) with different ratios. The sedimentation factor (SF) was calculated to quantify the extent of sedimentation by subtracting the final absorbance (A_t) from the initial absorbance (A_0) for each MHFs, as expressed in Eq. 2:

$$(\mathrm{SF}) = A_0 - A_t \tag{2}$$

To derive the percentage of sedimentation, the sedimentation factor (SF) was multiplied by 100 to express the extent of sedimentation, as shown in Eq. 3.

$$(\mathrm{SF})\% = \left(\frac{\text{Sedimentation factor}}{\text{Initial Absorbance}}\right) \times 100 \tag{3}$$

The objective is to determine the sedimentation percentage for each nanofluid, reflecting particle settling. Equation 4 calculates the percentage deviation from the average absorbance, using the most stable MHFs as a reference.

$$\text{Deviation} = \left(\frac{\text{Average Absorbance} - \text{Most Stable Average Absorbance}}{\text{Most Stable Average Absorbance}}\right) \times 100 \tag{4}$$

A photograph-capturing technique was employed to monitor sedimentation in MHF nanofluid samples. Photographs were taken immediately after preparation, 24-h later, and 30 days later. These sequential photographs allowed visual observation of particle settling and offered qualitative insights into the nanofluids' stability and sedimentation tendencies, complementing quantitative data from other measurements. This multi-technique approach enhances understanding of MHFs and their applications.

Thermoelectric conductivity of the MHFs

The thermoelectric conductivity (TEC) is behavior of the nanofluid that pertains to its potential utilization in electrically active environments, like PEM fuel cells, PV thermal systems among other energy systems. It is calculated using the equation provided by Zakaria et al. [36]

$$\mathrm{TEC} = \frac{5K_{nf}}{\sigma_{nf}K_{bf}} \tag{5}$$

where K_{nf} and σ_{nf} are the nanofluid thermal and electrical conductivity, respectively, and K_{bf} is the base fluid's thermal conductivity.

Machine learning approach

This study applied machine learning techniques to model and predict the thermal conductivity and viscosity of hybrid ferrofluids comprising water-based suspensions of Fe_3O_4, TiO_2, MgO, and ZnO nanoparticles. Modeling was conducted in a Python Jupyter Notebook environment using the Scikit-learn library using similar approach by Awe et al. [37, 38]. The dataset included temperature (T) and mixing ratios of the nanoparticles (Fe, Ti, Mg, Zn) as input features, while thermal conductivity (TC) and viscosity (Vis) served as target outputs. Data preprocessing involved cleaning, formatting, and structuring the variables into feature–target pairs.

Linear regression was used to establish relationships between the input features and target properties for each nanofluid composition. The models were trained and evaluated using fivefold cross-validation to ensure generalizability. Performance metrics such as R^2, mean squared error (MSE), and mean absolute error (MAE) were computed for both fitted and cross-validated results. Additionally, for thermal conductivity prediction, a random forest regressor was employed to assess feature importance.

Uncertainty analysis

The approach outlined in [39, 40] was utilized to estimate the uncertainty associated with key measured parameters, including dynamic viscosity (μ) and standard deviation (σ), by applying Eqs. (6) and (7). These uncertainties were determined with a 95% confidence level. Instrument precision was assessed based on bias errors, which reflect the accuracy limitations specified by the equipment manufacturer. The uncertainty in viscosity measurements was found to be ± 1.93%, while that of electrical conductivity measurements was ± 2.19%.

$$U_\mu = \sqrt{\left(\frac{\Delta m}{m}\right)^2 + \left(\frac{\Delta V}{V}\right)^2 + \left(\frac{\Delta T}{T}\right)^2 + \left(\frac{\Delta \mu}{\mu}\right)^2} \tag{6}$$

$$U_K = \sqrt{\left(\frac{\Delta m}{m}\right)^2 + \left(\frac{\Delta V}{V}\right)^2 + \left(\frac{\Delta T}{T}\right)^2 + \left(\frac{\Delta \sigma}{\sigma}\right)^2} \tag{7}$$

Results and discussion

Morphology of MHFs nanoparticles

The investigation of MHFs nanofluids, comprising Fe_3O_4 combined with TiO_2, MgO, and ZnO in varying proportions (80%, 60%, and 40%, for Fe_3O_4, and 20%, 40%, and 60%, for TiO_2, MgO, and ZnO, respectively), involved the analysis of their morphology and stability using transmission electron microscopy (TEM). The SEM images presented in Fig. 1 show the morphological behavior of the Fe_3O_4, TiO_2, (18 nm), TiO_2, (60 nm), MgO, and ZnO nanoparticles, respectively, was taken at a magnification of 100 KX, EHT of 2.0 kV, and at a scanning speed of 9 µm/s. The image in Fig. 1 (a) reveals that the Fe_3O_4 is a blend of small and large dispersed plate-like nanosheets. The image in Fig. 1 (b)-© shows that the TiO_2, (18 nm), TiO_2, (60 nm) MgO, and ZnO nanoparticles are all spherical in shape.

Quantitative estimation of the relative stability of the MHFs

The relative stability of the MHFs was assessed using three different comparative approaches for each sample at varying mixing ratios. These approaches included physical sedimentation inspection over time, absorbance against wavelength,

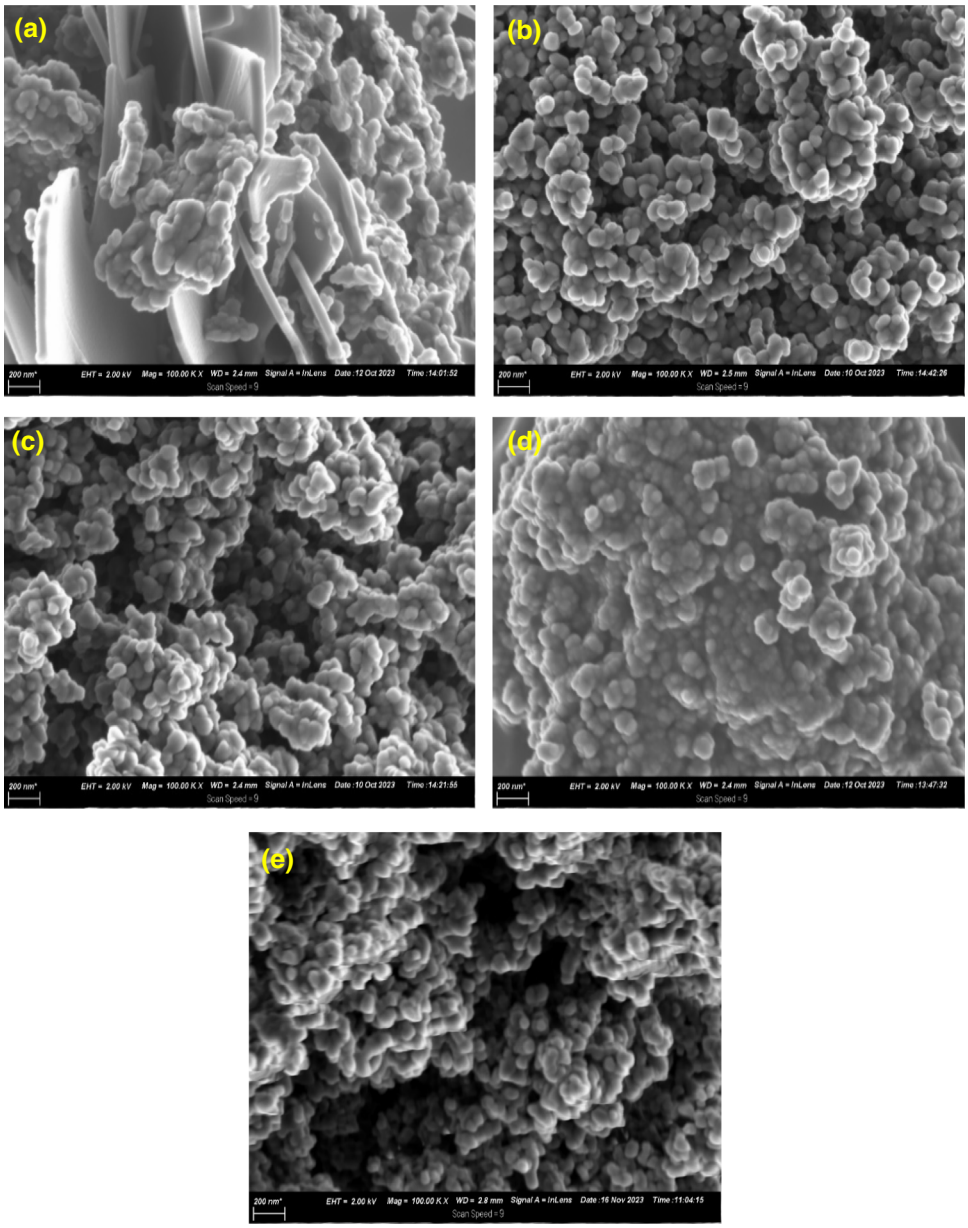

Fig. 1 Morphological result of the SEM **a** Fe_3O_4, **b** TiO_2 (18 nm), **c** TiO_2 (60 nm), **d** MgO, & © ZnO

and thermal conductivity over time. Pictures of the physical inspection, conducted immediately after the preparation of the MHFs and after 30 days of shelf life, are presented in Fig. 2a & b and c & d, respectively. The physical sedimentation inspection reveals that only slight sedimentation occurred after 30 days, indicating that the nanofluids remain stable over an extended period.

Absorbance of MHF with wavelength

The hybridization mixing ratio denotes the proportion of different components in the nanofluid, specified as 80:20, 60:40, and 40:60 for various combinations of Fe_3O_4/TiO_2 -DIW, Fe_3O_4/MgO-DIW, and Fe_3O_4/ZnO-DIW. Measurements were taken over a range of wavelengths, spanning from 200 to 280 nm with a 10-nm interval, followed by 281–300 nm with a 1-nm interval. Figure 3 provides valuable insights into the relationship between absorbance values and hybridization mixing ratios, shedding light on sedimentation tendencies.

In the case of Fe_3O_4/TiO_2(18 nm)-DIW (80:20), absorbance values consistently rise across wavelengths, indicative of stability with minimal fluctuations. A similar pattern of stability and dispersion is maintained by Fe_3O_4/TiO_2(18 nm) -DIW (80:20). On the other hand, Fe_3O_4/MgO-DIW (80:20) starts with lower absorbance values but gradually increases, suggesting reasonable stability. Fe_3O_4/ZnO-DIW (80:20) follows a comparable trend but might indicate slight aggregation or sedimentation, given the rising absorbance.

However, for 60:40 and 40:60 HMR MHFs' trend shows increasing absorbance values with a potential for particle aggregation or sedimentation. This tendency is more pronounced at 60:40 and 40:60 ratios. It becomes evident that hybridization mixing ratios significantly influence stability, with higher Fe_3O_4 ratios promoting stability and other materials like MgO or ZnO potentially contributing to destabilization. These observed trends reflect the complex interplay between nanoparticle interactions, surface chemistry, and concentration.

Influence of HMR and particle size on sedimentation factor of MHFs

The sedimentation factor (%) for the MHFs at various hybridization mixing ratios (HMR) was calculated using Eq. 3, and the respective sedimentation factors for all the MHFs are presented in Table 2. Generally, the 80:20 hybridization mixing ratio exhibited the least sedimentation factor for most MHFs, except in the case of Fe_3O_4/MgO/DIW. Additionally, the results indicate that Fe_3O_4/TiO_2 (60nm)-DIW with a hybridization mixing ratio of 80:20 had the lowest percentage sedimentation factor at 0.0667, suggesting superior stability compared to the others. Both TiO_2-based hybrid ferrofluids, whether 18nm or 60nm, displayed relatively low sedimentation factors. Interestingly, the larger TiO2 (60nm) exhibited a lower sedimentation factor compared to the smaller TiO_2 (18nm) hybrid ferrofluid. Conversely, the Fe_3O_4/MgO/DIW (60:40) hybrid ferrofluid showed the least stability, as evidenced by the largest sedimentation factor of 4.119%. Thus, both the hybridization mixing ratio and particle size are crucial factors for achieving the desired stability in MHF.

Thermal conductivity of the MHFs

Impact of temperature, shelf life, and HMR on nanofluid thermal conductivity stability

To evaluate the suitability of hybrid magnetic nanofluids (HMFs) for heat transfer applications, we examined the stability of their thermal conductivity values within a temperature range of 10–50°C, over a shelf life of 30 days. This

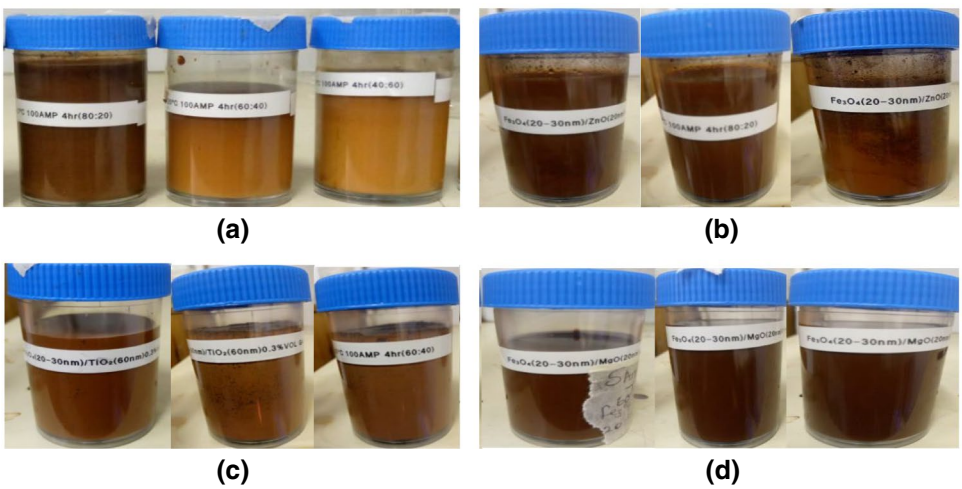

Fig. 2 Physical observing sedimentation in MHFs nanofluid samples **a** Fe_3O_4(20-30 nm)/Ti O_2(18 nm), **b** Fe_3O_4(20–30 nm)/ ZnO(20 nm), **c** Fe_3O_4(20-30 nm)/ Ti O_2(60 nm) & **d** Fe_3O_4 (20–30 nm)/MgO(20 nm) various hybrid after 30 days

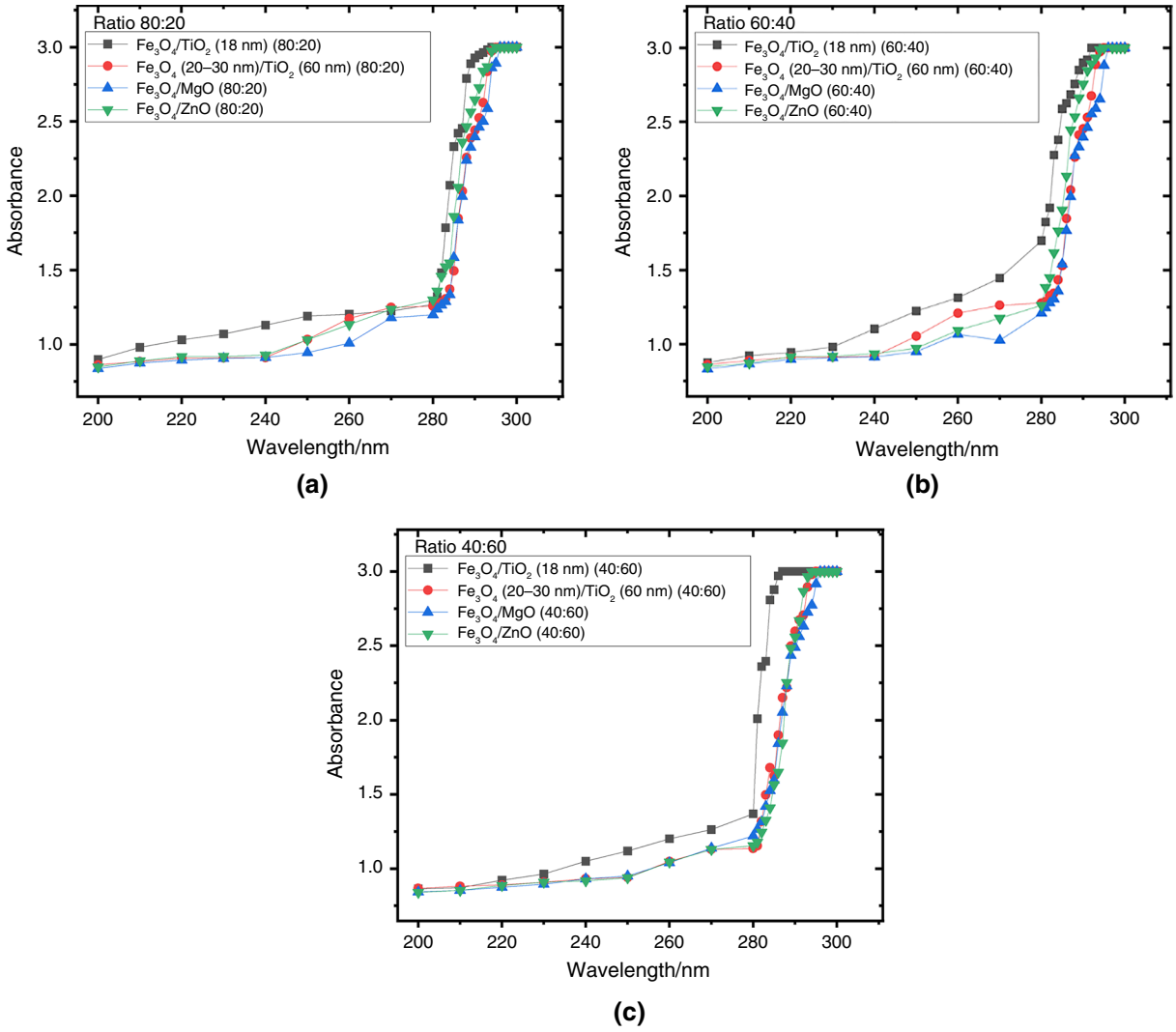

Fig. 3 UV–Vis spectrum of magnetic hybrid nanofluid dispersed in DIW with ratio **a** 80:20, **b** 60:40, and **c** 40:60

Table 2 Sedimentation factor for the different MHFs

S/n	MHF	HMR	Peak wavelength /nm	Sedimentation factor /%
1	Fe_3O_4/TiO_2(18*nm*)/DIW	80:20	293	0.5690
2	Fe_3O_4/ TiO_2(60 nm)/DIW	80:20	295	0.0667
3	Fe_3O_4/MgO/DIW	80:20	295	3.6990
4	Fe_3O_4/ZnO/DIW	80:20	294	0.8812
5	Fe_3O_4/TiO_2(18*nm*)/DIW	60:40	291	2.7490
6	Fe_3O_4/ TiO_2(60 nm)/DIW	60:40	294	0.9290
7	Fe_3O_4/MgO/DIW	60:40	295	4.1190
8	Fe_3O_4/ZnO/DIW	60:40	294	0.4020
9	Fe_3O_4/TiO_2(18*nm*)/DIW	40:60	280	1.0100
10	Fe_3O_4/ TiO_2(60 nm)/DIW	40:60	294	0.7050
11	Fe_3O_4/MgO/DIW	40:60	295	2.8800
12	Fe_3O_4/ZnO/DIW	40:60	294	0.7050

assessment involved different hybridization mixing ratios (HMRs), including 80:20, 60:40, and 40:60 for four distinct HMF types: Fe_3O_4/TiO_2(18 nm)/DIW, Fe_3O_4/TiO_2(60nm)/DIW, Fe_3O_4/MgO(20nm)/DIW, and Fe_3O_4/ZnO (20nm)/DIW. Figure 4 illustrates the thermal conductivity values of these MHFs at a 0.3% volume concentration.

Across all cases, the effect of temperature on thermal conductivity values followed a common trend: an increase in thermal conductivity with rising fluid temperature. Over 24 h, we assessed the stability of thermal conductivity measurements, revealing minor differences between values obtained immediately after preparation and those taken 30 days later. This indicates that the nanofluids consistently maintained their thermal conductivity over the 30 days, with average percentage deviation values demonstrating this stability.

The results highlighted the thermal conductivity stability with respect to different hybridization mixing ratios

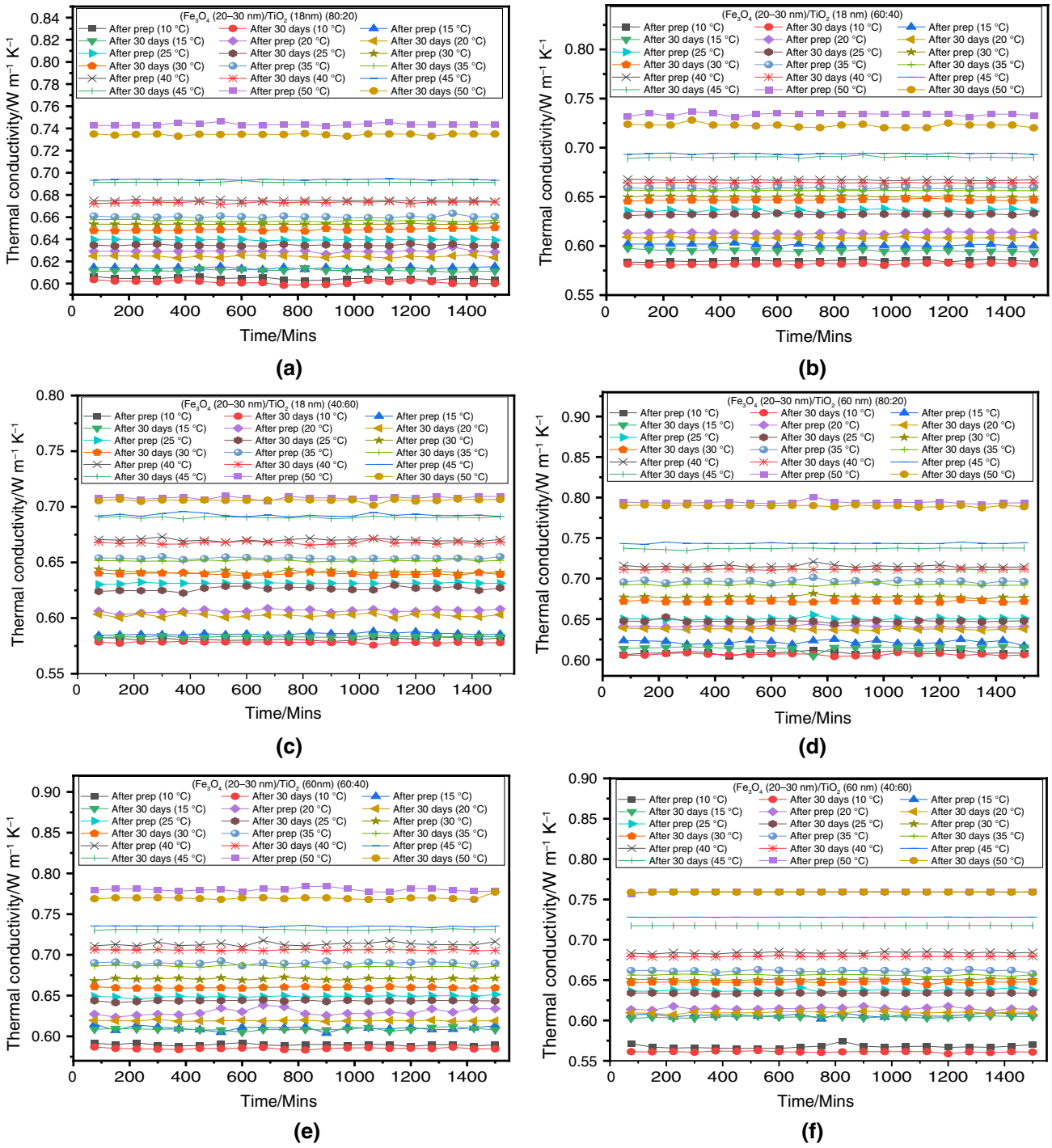

Fig. 4 Thermal conductivity of MHFs as a function of temperature, shelf life, and time for **a** Fe_3O_4/TiO_2 (18 nm)/DIW (80:20), **b** Fe_3O_4/ TiO_2 (18 nm)/DIW (60:40), **c** Fe_3O_4/ TiO_2 (18 nm)/DIW (40:60), **d** Fe_3O_4/ TiO_2 (60 nm)/DIW (80:20), e Fe_3O_4/ TiO_2 (60 nm)/DIW (60:40), **f** Fe_3O_4/ TiO_2 (60 nm)/DIW (40:60), **g** Fe_3O_4/ MgO (20 nm)/DIW (80:20), **h** Fe_3O_4/ MgO (20 nm)/DIW (60:40) **i** Fe_3O_4/ MgO (20 nm)/DIW (40:60), **j** Fe_3O_4/ ZnO (20 nm)/DIW (80:20), **k** Fe_3O_4/ ZnO (20 nm)/DIW (60:40), **l** Fe_3O_4/ ZnO (20 nm)/DIW (40:60)

(80:20, 60:40, and 40:60). MHFs with an HMR of 80:20 consistently displayed remarkable stability, characterized by the lowest percentage deviations and standard deviation (STDEV) percentages across varying temperatures. The highest percentage deviation for the 80:20 hybrid was 0.39% at 15 °C, while the lowest was 0.16%, and the lowest STDEV was 0.08% at 40 °C. In contrast, the 60:40 hybrid exhibited the highest percentage deviation of 0.86% at 30 °C, and the

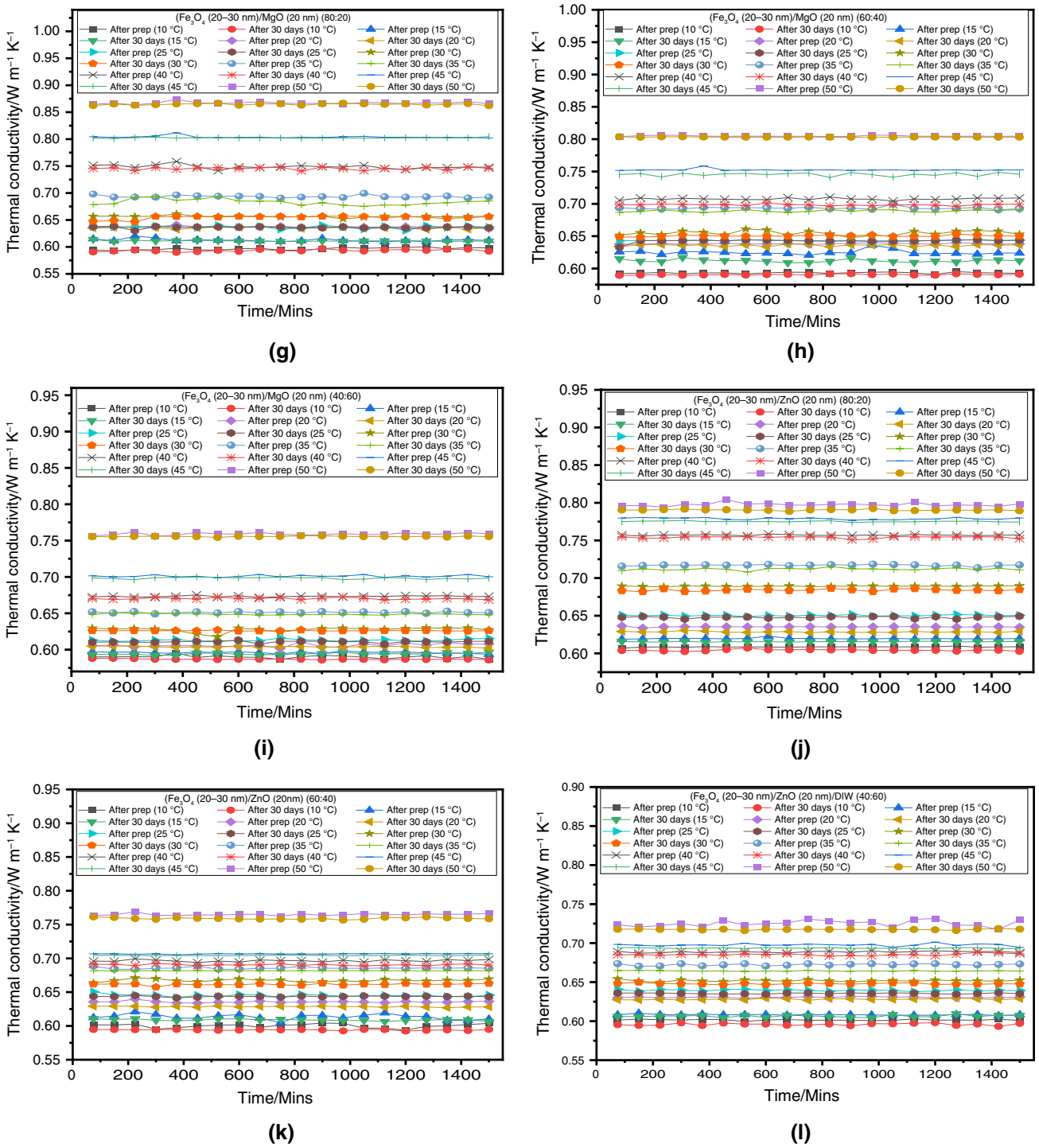

Fig. 4 (continued)

lowest was 0.52% at 25 °C. For the 40:60 hybrid, the highest percentage deviation was 0.67% at 20 °C, and the lowest was 0.23%.

These findings highlighted the substantial impact of hybridization mixing ratios on the stability of thermal conductivity measurements, with HMFs employing an 80:20 hybrid consistently outperforming others regarding stability and thermal conductivity. The choice of the hybridization mixing ratio significantly influences the stability and reliability of thermal conductivity measurements, with the 80:20 hybrid emerging as the most suitable option for heat transfer scenarios. Importantly, the 80:20 hybrid consistently

exhibited lower percentage deviations, indicating superior stability and consistency in thermal conductivity measurements compared to other hybrids. The 80:20 hybrid showed consistent stability from 10°C to 50°C, crucial for heat transfer applications.

Influence of temperature and hybridization mixing ratio on thermal conductivity of the MHFs

The plots in Figs. 4a–f and 5a & b vividly demonstrate the impact of temperature on the thermal conductivity of various MHFs in comparison with DIW at different hybridization mixing ratios (HMRs). Let us break down the findings for each type of MHF.

For Fe_3O_4/ TiO_2 (18nm)-DIW MHFs immediately after preparation:

- (80:20) HMR: At lower temperatures (10–25 °C), the enhancement ranged from 4.20% to 5.23%. At higher temperatures (30–45 °C), it peaked at around 9.37%.
- (60:40) HMR: This ratio showed enhancements from 0.87% at 10 °C to 8.79% at 45 °C.
- (40:60) HMR: Enhancements ranged from 0.24% at 10 °C to 7.49% at 45 °C. These results underscore the effectiveness of the (80:20) HMR in improving thermal conductivity immediately after preparation.

After 30 days of preparation, the (80:20) HMR continued to show enhancements, ranging from 4.00% to 7.22% across the temperature range. The (60:40) HMR exhibited enhancements from 0.29% at 10 °C to 6.19% at 45°C, while the (40:60) HMR recorded enhancements between 0.29% and 5.41%. The (80:20) HMR remained the most effective choice for enhancing thermal conductivity, even after 30 days of preparation, particularly at elevated temperatures.

For Fe_3O_4/TiO_2(60 nm)-DIW MHFs:

- (80:20) HMR: The enhancements immediately after preparation ranged from 5.00% at 10 °C to 17.17% at 45 °C. After 30 days, enhancements remained substantial, varying from 4.57% at 10°C to 16.45% at 45°C.

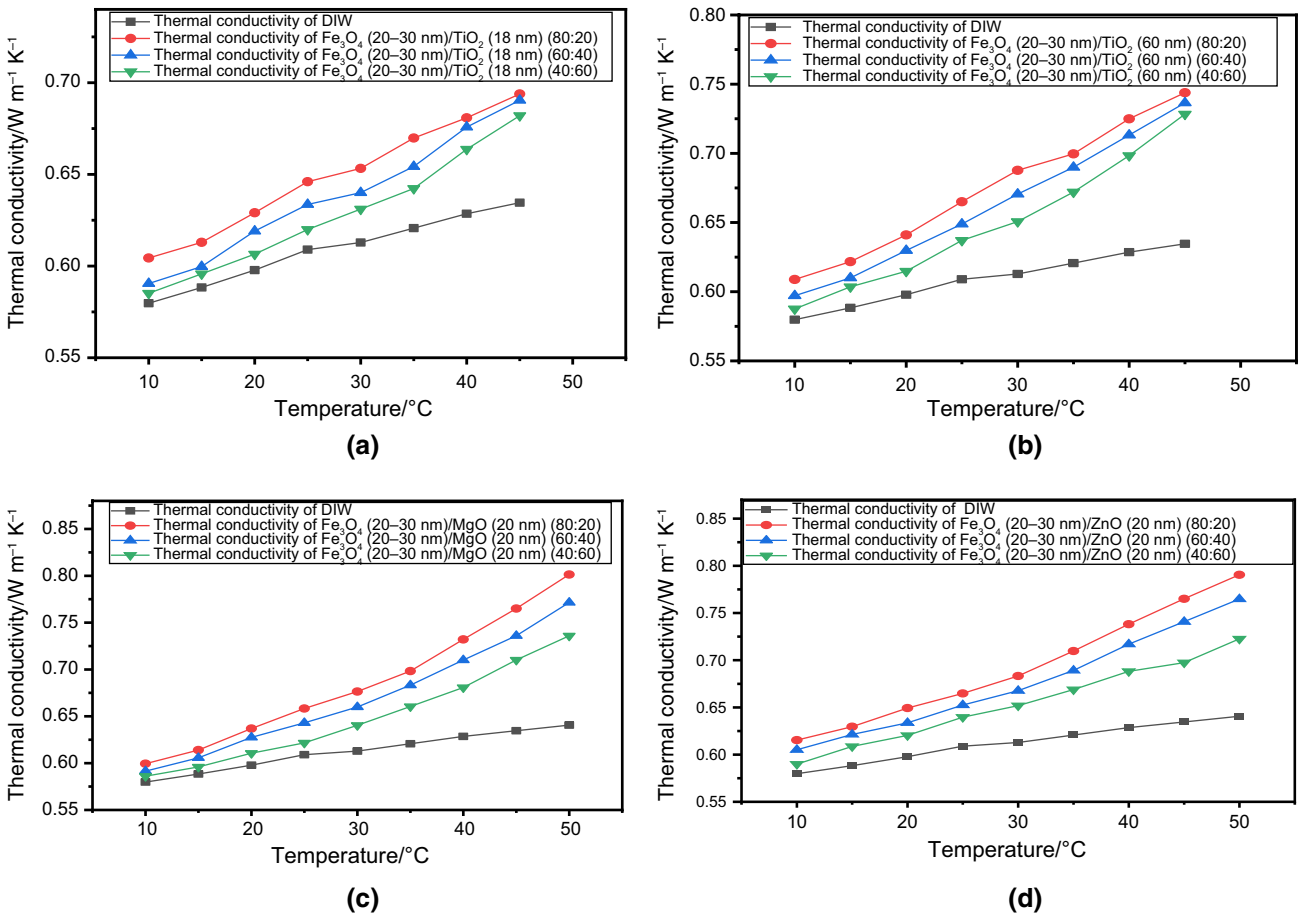

Fig. 5 Thermal conductivity measured values in comparison with HMR as function of temperature for **a** Fe_3O_4/TiO_2(18 nm), **b** Fe_3O_4/TiO_2 (60 nm), **c** Fe_3O_4/MgO, **d** Fe_3O_4/ZnO

- (60:40) HMR: Initially, enhancements ranged from 1.71% at 10 °C to 16.04% at 45 °C. After 30 days, while there was a slight decrease, enhancements remained substantial, varying from 0.90% at 10 °C to 15.40% at 45 °C.
- (40:60) HMR: Enhancements ranged from 1.21% at 10 °C to 14.76% at 45 °C immediately after preparation, with values between 0.22% at 10 °C and 13.71% at 45 °C after 30 days.

These findings affirm the effectiveness of the (80:20) HMR in improving thermal conductivity, particularly at higher temperatures.

For Fe_3O_4/MgO-DIW MHFs, the percentage enhancements for the:

- (80:20) HMR immediately after preparation ranged from approximately 3.26% at 10 °C to about 27.92% at 50 °C.
- (60:40) HMR, enhancements varied from approximately 2.03% at 10 °C to 25.91% at 50°C.
- (40:60) HMR recorded enhancements ranging from around 1.29% at 10 °C to approximately 21.04% at 50 °C.

The data underscore the (80:20) HMR as the most effective choice for enhancing thermal conductivity, both immediately after preparation and after 30 days, across varying temperatures.

For Fe_3O_4/ZnO-DIW MHFs, the percentage enhancements for the:

- (80:20) HMR had the best thermal conductivity among other MHFs and HMRs; it has thermal conductivity value of 0.793 W/m.K at 50 °C and its percentage enhancement ranged from about 4.23% at 10 °C to about 31.28% at 50 °C.
- (60:40) HMR, enhancements varied from approximately 3.86% at 10 °C to 29.76% at 50 °C.
- (40:60) HMR recorded enhancements ranging from around 1.75% at 10 °C to approximately 27.46% at 50 °C.

These results consistently demonstrate that the (80:20) HMR outperforms the (60:40) and (40:60) ratios in enhancing thermal conductivity, both immediately after preparation and after 30 days, across varying temperatures. This makes the (80:20) HMR an excellent choice for applications demanding efficient forced convection heat transfer.

Influence of particle size on the thermal conductivity of the MHFs

The results illustrated in Figs. 4a–f and 5a & b show that MHFs containing TiO_2 (60 nm) exhibited superior stability and thermal conductivity compared to their counterparts with TiO_2 (18 nm) across various hybridization ratios. This distinction in particle size significantly influences thermal conductivity enhancement, as observed with TiO_2. Larger nanoparticles, due to their greater surface area, foster enhanced conductive heat transfer interactions within the particles and between the particles and the base fluid (DIW) [41]. This phenomenon can account for the higher percentage of enhancements detected in Fe_3O_4/TiO_2 (60nm)-DIW nanofluids in comparison with those containing Fe_3O_4/TiO_2 (60 nm)-DIW MHFs. In summary, the particle size of TiO_2 nanoparticles substantially impacts the thermal conductivity enhancement of these nanofluids, with smaller particles potentially offering more significant improvements in heat transfer properties.

Thermal conductivity model

This section presents the correlation analysis between thermal conductivity (K) and its influencing variables: temperature (T), volume fraction (ϕ), and the percentage or ratio of individual metal oxide nanoparticles, namely iron(III) oxide (Fe), titanium oxide (Ti), magnesium oxide (Mg), and zinc oxide (Zn). A linear regression modeling approach was implemented within a Python Jupyter Notebook environment, using fivefold cross-validation to ensure robust and generalized performance assessment.

As a baseline validation step, the thermal conductivity of deionized water (DIW) was modeled and compared against experimentally measured values and benchmark correlations from Yunus and Çengel [50] and Popiel and Wojtkowiak [49]. As illustrated in Fig. 6, the DIW regression model demonstrated excellent agreement with both measured data and literature values across the 10–50 °C range. The model achieved a high R2 value of 0.9839 and an extremely low mean squared error (MSE) of 0.000002,

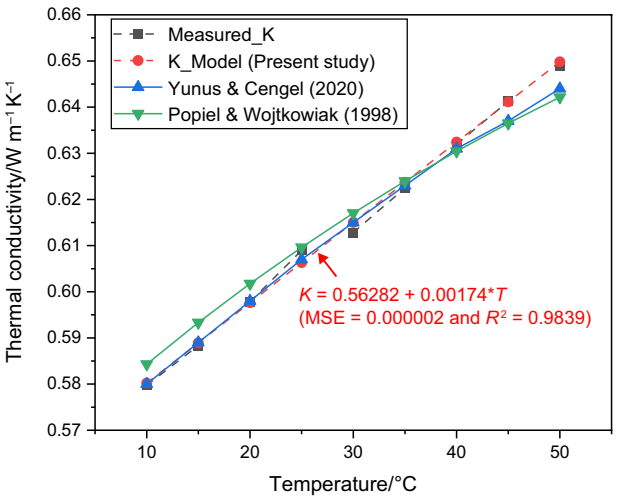

Fig. 6 Validation of thermal conductivity model

confirming its reliability and establishing confidence in the modeling framework before extending it to hybrid ferrofluid systems.

The developed regression models for hybrid nanofluids Fe_3O_4–TiO_2 (18 nm), Fe_3O_4–MgO, Fe_3O_4–ZnO, and Fe_3O_4 –TiO_2 (60 nm) is summarized in Table 3 and visually presented in Fig. 7. Model performance was assessed using the R2 and MSE metrics, which indicated that the linear models successfully captured the variation in thermal conductivity with changes in temperature and nanoparticle composition. High R2 values and low MSE scores across most systems suggest that the linear models exhibit strong predictive accuracy, with predictions closely matching experimental values. However, systems with more complex particle interactions (e.g., Fe_3O_4–TiO_2 at 60 nm) showed relatively lower R2, indicating potential nonlinear behavior that might benefit from more advanced modeling approaches.

To further assess the influence of individual variables on thermal conductivity, a random forest regressor was employed for feature importance analysis due to its nonlinear modeling capability and strong performance. As shown in Fig. 8, **t**emperature (T) emerged as the most influential factor across all hybrid ferrofluid systems. The volume fraction (ϕ) also showed a consistent and moderately strong effect, reflecting its critical role in enhancing heat transfer pathways. Among the elemental components, Zn contributed more significantly than Ti or Mg, while Fe had a moderate influence. Notably, the overall mixing ratio (MR) exhibited the least importance, suggesting that while compositional presence matters, the thermal response is more strongly

Table 3 Thermal conductivity correlations and performance metrics

Fluid	Equation	R^2/ %	MSE
DIW	K = 0.00174 T + 0.56282	98.39	0.000002
Fe_3O_4–TiO_2 (18 nm)/DIW	K = 0.0027 T + 0.032 Fe − 0.032 Ti + 0.105 ϕ + 0.5161	80.23	0.0003
Fe_3O_4–MgO/DIW	K = 0.0052 T + 0.1026 Fe − 0.1026 Mg + 0.0434 ϕ + 0.4740	87.27	0.0008
Fe_3O_4–ZnO/DIW	K = 0.0031 T + 0.0176 Fe − 0.0176 Zn + 0.1508 ϕ + 0.5040	87.59	0.0003
Fe_3O_4–TiO_2 (60 nm)/DIW	K = 0.0047 T + 0.0275 Fe − 0.0275 Ti + 0.1747 ϕ + 0.4586	56.99	0.0030

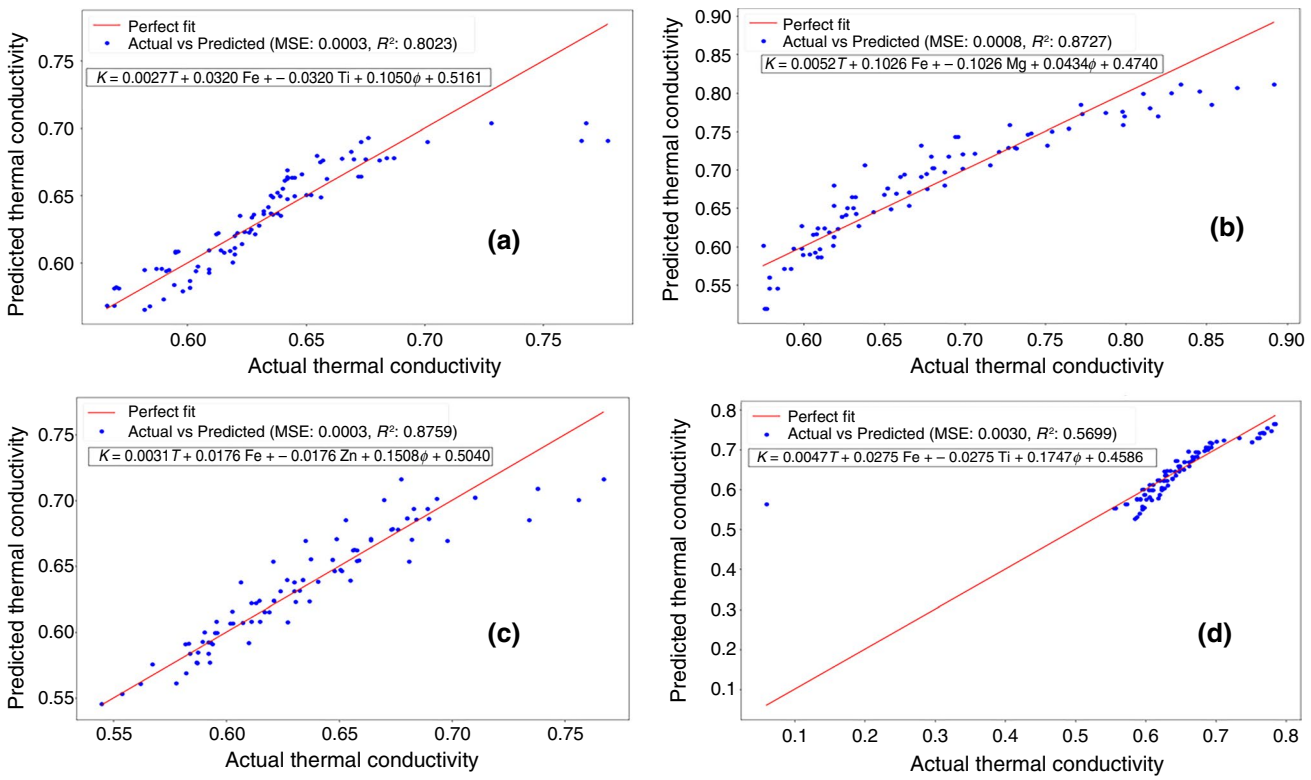

Fig. 7 Linear regression model predictions for thermal conductivity (K) of **a** Fe_3O_4-TiO_2 (18 nm), **b** Fe_3O_4-MgO, **c** Fe_3O_4-ZnO, and (d) Fe_3O_4–TiO_2 (60 nm) DIW hybrid ferrofluids

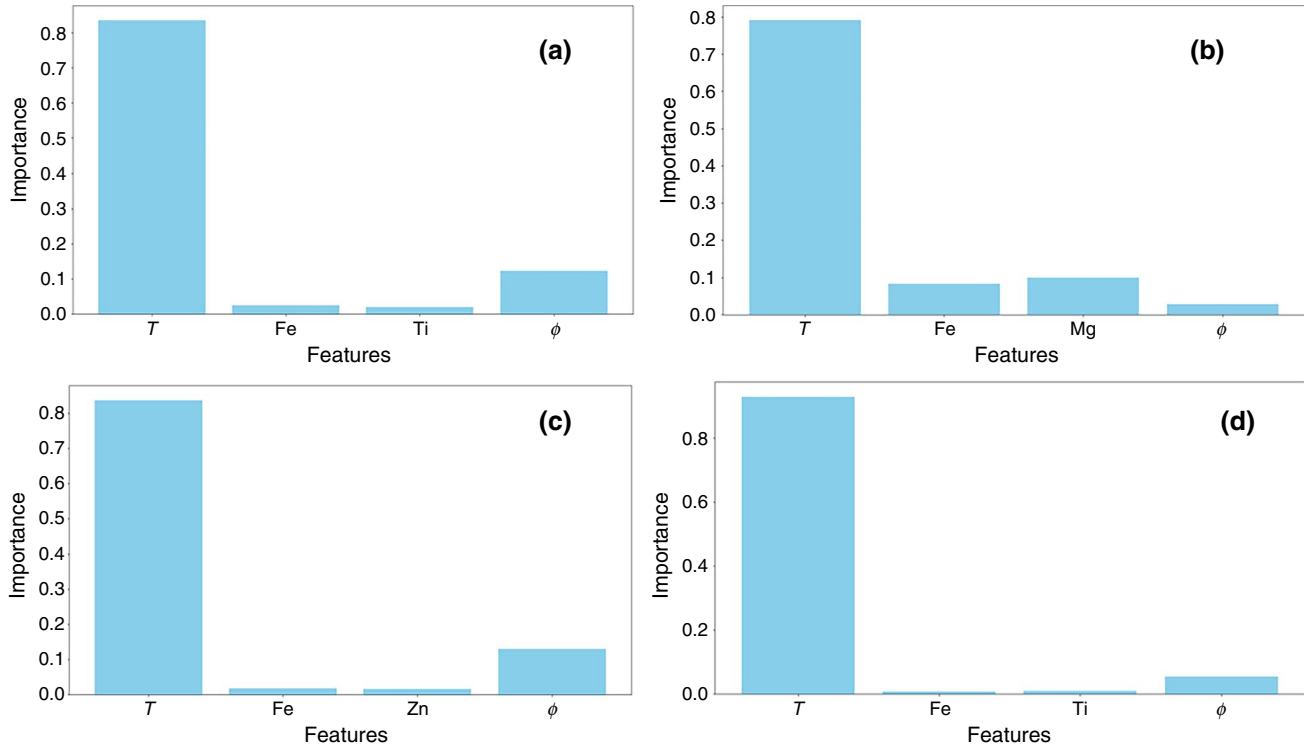

Fig. 8 Feature importance analysis for predicting thermal conductivity of **a** Fe_3O_4-TiO_2 (18 nm), **b** Fe_3O_4-MgO, **c** Fe_3O_4-ZnO and (d) Fe_3O_4 -TiO_2 (60 nm) DIW hybrid ferrofluids

governed by temperature and particle concentration than by relative proportions.

Influence of temperature and HMR on the electrical conductivity of the MHFs

Electrical conductivity refers to the property of an aqueous solution that allows it to conduct electric current when subjected to a potential difference. When nanoparticles are introduced into base fluids, forming nanofluids, the electrical conductivity of these fluids is notably enhanced. This enhancement is attributed to the increased mobility of electric charges facilitated by the dispersion of nanoparticles. The experimental results, presented in Figs. 9 and 10, illustrate the relationship between temperature and the electrical conductivity of the different magnetic hybrid nanofluids (MHFs) considered in this study, each with varying hybridization mixing ratios (HMRs) compared to deionized water (DIW).

In Fig. 9a, the effect of temperature on the electrical conductivity of Fe_3O_4/TiO_2(18 nm)-DIW MHFs with different HMRs (80:20, 60:40, and 40:60) is demonstrated. The 80:20 HMR exhibited the highest electrical conductivity, recording a value of 4.25 and a remarkable percentage enhancement of 972.93% at 45°C compared to DIW. Similarly, the 60:40 HMR displayed an impressive percentage enhancement of 964.82%, making it the top-performing HMR. The 40:60 HMR showed an enhancement of 479.45%. This highlights the significant influence of HMRs on electrical conductivity, especially at elevated temperatures.

Figure 9b showcases the impact of temperature on the electrical conductivity of Fe_3O_4/ Ti O_2(60nm)-DIW MHF, also featuring varying HMRs. All ratios exhibited consistent increases in electrical conductivity with rising temperature, demonstrating a positive correlation. The 80:20 HMR had the highest electrical conductivity, with an enhancement of 377.12%. The 60:40 ratio showed a 333.35% enhancement, while the 40:60 ratio displayed an enhancement of 311.28%.

The disparity in electrical conductivity between larger (60nm) and smaller (18nm) TiO_2 nanoparticles, as shown in Fig. 10, may be attributed to differences in nanoparticle density. Denser nanoparticles could hinder charge carrier mobility, leading to decreased conductivity due to increased scattering [42–44]. However, it is worth noting that despite lower electrical conductivity, the 60-nm nanoparticles exhibit higher thermal conductivity, indicating divergent mechanisms at play. Further investigation into the role of nanoparticle density in electrical conductivity in magnetic hybrid nanofluids (MHNFs) is warranted, as it involves an intricate interplay between particle size, density, and charge carrier behavior. In Figs. 6, 9c, the dataset illustrates electrical conductivity values across various HMRs of Fe_3O_4/

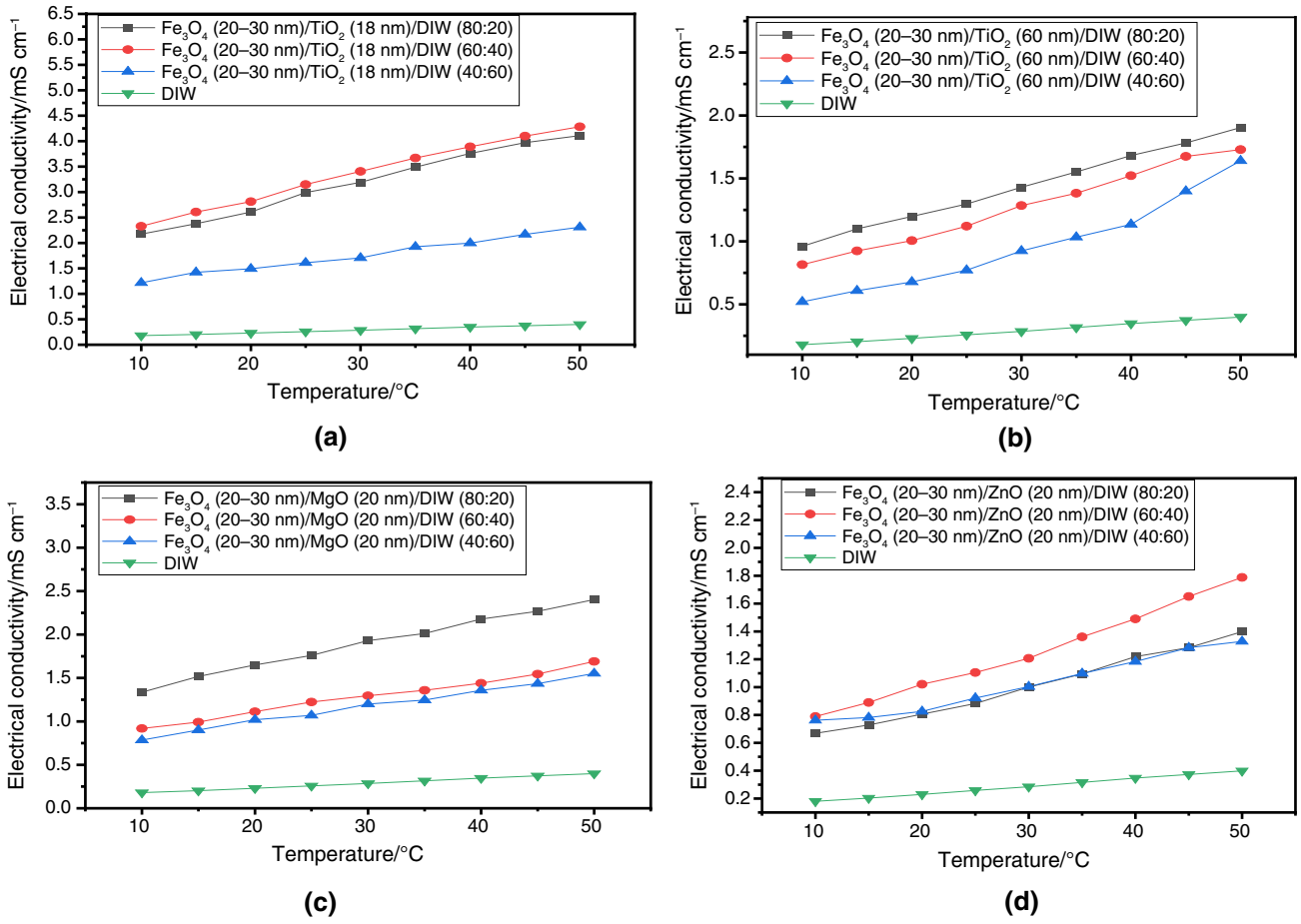

Fig. 9 Electrical conductivity of hybrid nanofluids against temperature at different hybridization mixing ratios of **a** Fe_3O_4/TiO_2(18 nm), **b** Fe_3O_4/TiO_2(60 nm), **c** Fe_3O_4/MgO, **d** Fe_3O_4/ZnO

MgO-DIW MHF at different temperatures, reiterating the consistent positive correlation between temperature and electrical conductivity. Notably, the 80:20 HMR demonstrated the highest electrical conductivity, featuring a 502.76% enhancement. The 60:40 HMR had a maximum electrical conductivity of 298.00%, while the 40:60 HMR exhibited an enhancement of 289.22% compared to DIW.

The results in Fig. 9d present the electrical conductivity values of Fe_3O_4/ZnO-DIW MHFs at varying temperatures and various HMRs. An analysis of this dataset reveals that the relationship between temperature and electrical conductivity remains consistent. As temperature increases, electrical conductivity consistently rises across all HMRs. Notably, in contrast to previous results, the 60:40 HMR exhibits the highest electrical conductivity, reaching 1.803 mS/cm with an impressive enhancement of 351.88% compared to DIW. The 80:20 HMR records a value of 1.3986 mS/cm, featuring a percentage enhancement of 250.38%. Meanwhile, the 40:60 hybridization mixing ratio achieves a maximum electrical conductivity of 1.3286 mS/cm, with a percentage enhancement of 232.08%.

These findings notably surpass previous research. For instance, Bagheli et al. [45] reported an electrical conductivity value of 1.90 mS/cm for a 0.6 vol% Fe_3O_4/water nanofluid at 60 °C. Giwa et al. [16] observed an electrical conductivity range of 1.127–1.265 mS/cm for a 0.1 vol% AL_2O_3/MWCNT (80:20)-DIW nanofluid at 50 °C. In contrast, Giwa et al. [46] found an electrical conductivity of 6.40–4.570 mS/cm for a 0.75 vol% AL_2O_3-Fe_2O_3 (75:25)/DIW hybrid nanofluid at 50 °C. Another study by Giwa et al. [24] reported an electrical conductivity value of 4.319 mS/cm for an MWCNT-Fe_2O_3 (20:80)/DIW hybrid nanofluid. These comparisons shed light on the intricate interplay of parameters and underscore the unique contribution of the current study to the understanding of electrical conductivity in hybrid nanofluids.

Influence of temperature on pH of the MHFs

The pH level of a nanofluid indicates its degree of acidity or alkalinity, which, in the case of magnetic hybrid nanofluids (MHFs), can influence the surface charge of the

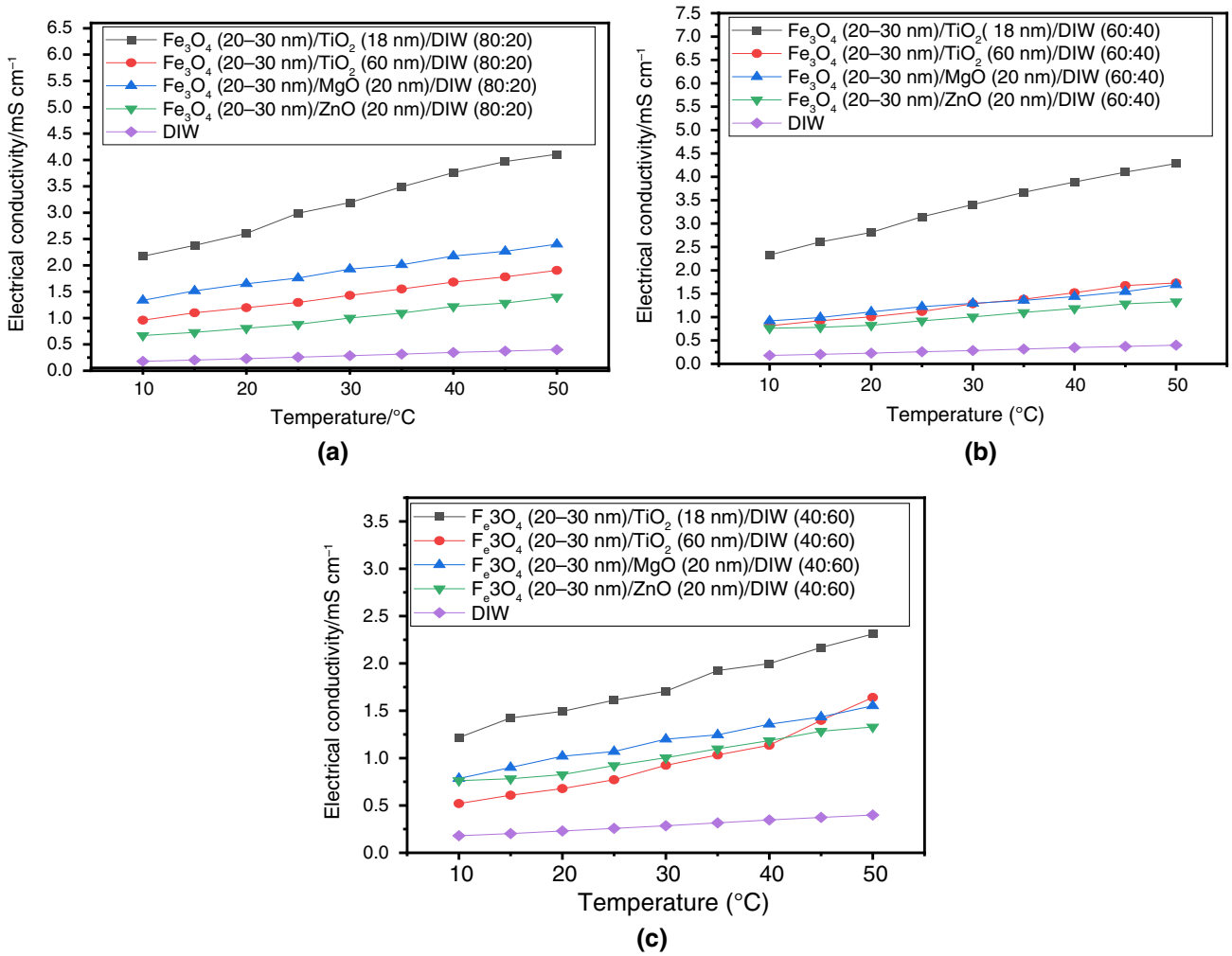

Fig. 10 Comparison of electrical conductivity of MHFs @ **A** 80:20, **B** 60:40, and **C** 40:60 with respect to temperatures

nanoparticles within the MHF. This surface charge, often a result of functional groups on the nanoparticle surface, plays a crucial role in stabilizing the nanofluid using electrostatic repulsion. In this section, we explore the effect of temperature on the pH of MHFs with hybridization mixing ratios (HMRs) of 80:20, 60:40, and 40:60, all with a 0.3 vol% concentration [11, 47].

As depicted in Fig. 11, the relationship between pH and temperature is examined. Generally, the pH levels of the MHFs exhibit a slight decrease as the temperature rises from 10 to 50 °C, maintaining a 0.3 vol% concentration throughout. In the case of all the MHFs considered, they tend to be more alkaline. However, both Fe_3O_4/TiO_2(18nm)-DIW and Fe_3O_4/TiO_2(60 nm)-DIW MHNFs consistently demonstrate relatively lower pH values across different HMRs, as shown in Fig. 9a–c. Conversely, the Fe_3O_4/MgO-DIW MHF exhibits the highest pH value, indicating a more acidic nature. The pH value remains consistent across various HMRs as temperature increases.

Viscosity of the MHFs

Experimental viscosity results

In this section, we examine the impact of temperature on the viscosity of various MHFs, including Fe_3O_4/TiO_2 (18nm)-DIW, Fe_3O_4/,TiO_2(60nm)-DIW, Fe_3O_4/MgO-DIW, and Fe_3O_4/ZnO-DIW MHFs. These MHFs have different hybrid mixing ratios (HMRs) of 80:20, 60:40, and 40:60, all with a 0.3 vol% concentration. Generally, the viscosity of all the MNFs decreases as the temperature rises, following the conventional theoretical trend for fluid viscosity. The viscosity measurement approach used in this study is depicted in Fig. 12, as described in the previous section.

As illustrated in Fig. 13, the Fe_3O_4/MgO-DIW MHF exhibits the highest viscosity among all the nanofluids considered for various mixing ratios. Conversely, the Fe_3O_4/ZnO-DIW MHFs consistently show the lowest viscosity values across the board, with a viscosity value of

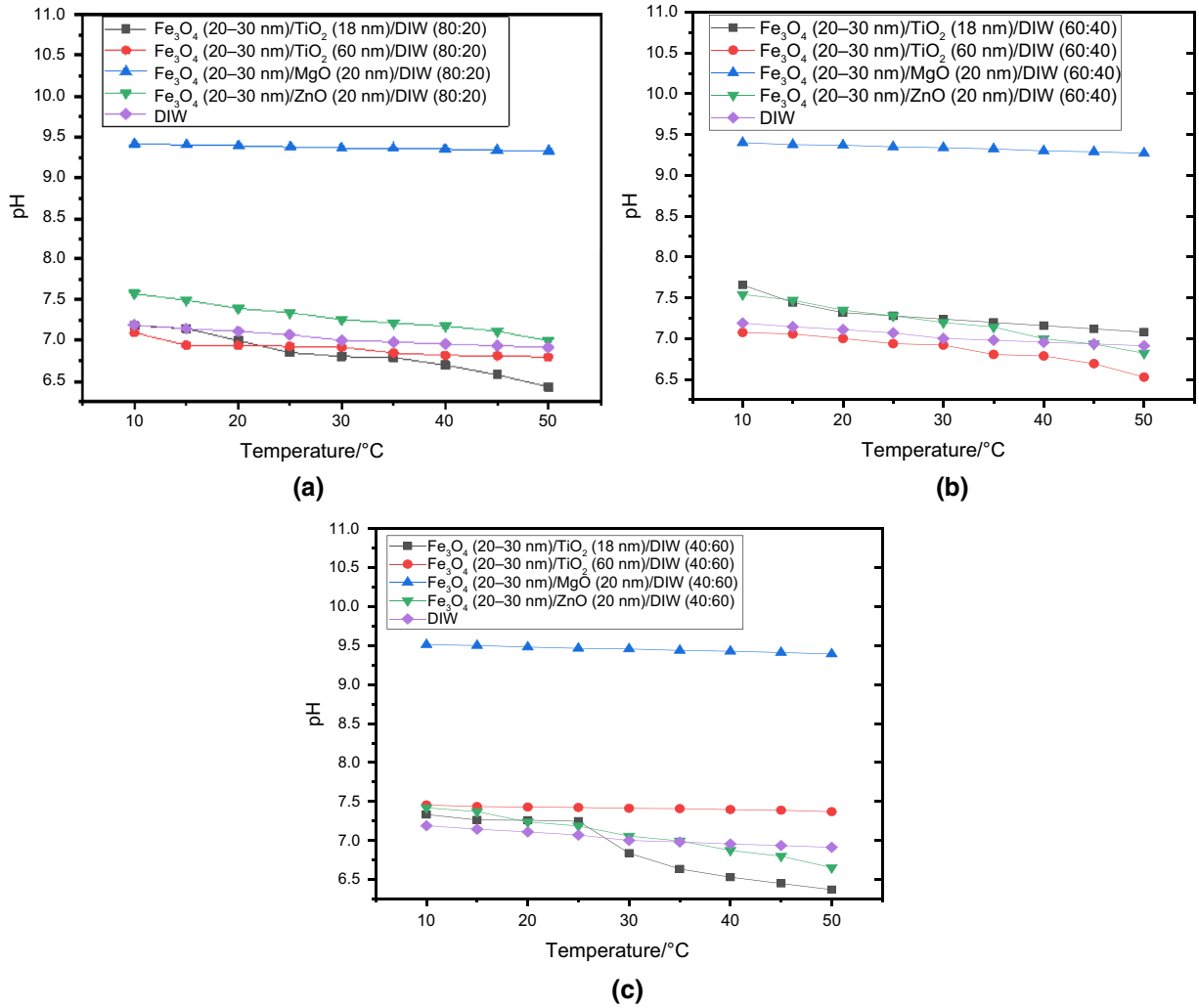

Fig. 11 pH of MHFs/DIW with **a** 80:20, **b** 60:40, and **c** 40:60 at different temperatures

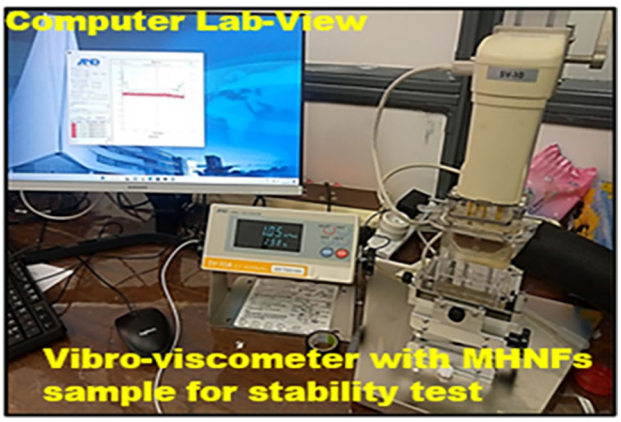

Fig. 12 Visual representation of viscosity measurement

1.62 mPa.S at 10 °C and 0.995 mPa.S at 50 °C. Its 60:40 HMR tends to exhibit higher viscosity, whereas the 80:20 HMR demonstrates the lowest viscosity for all the MHFs studied.

It is essential to note that higher viscosity in MHFs impacts the heat transfer behavior of the fluid by increasing frictional resistance to flow. This, in turn, leads to higher pressure drop and poses challenges for heat transfer efficiency [48]. The significant increase in viscosity observed in the Fe_3O_4/MgO-DIW MHF may render it impractical for heat transfer systems due to the high pressure drop, which implies a greater demand for pump power. Consequently, when selecting nanofluids, there should be a careful balance between thermal conductivity enhancement and the associated increase in viscosity.

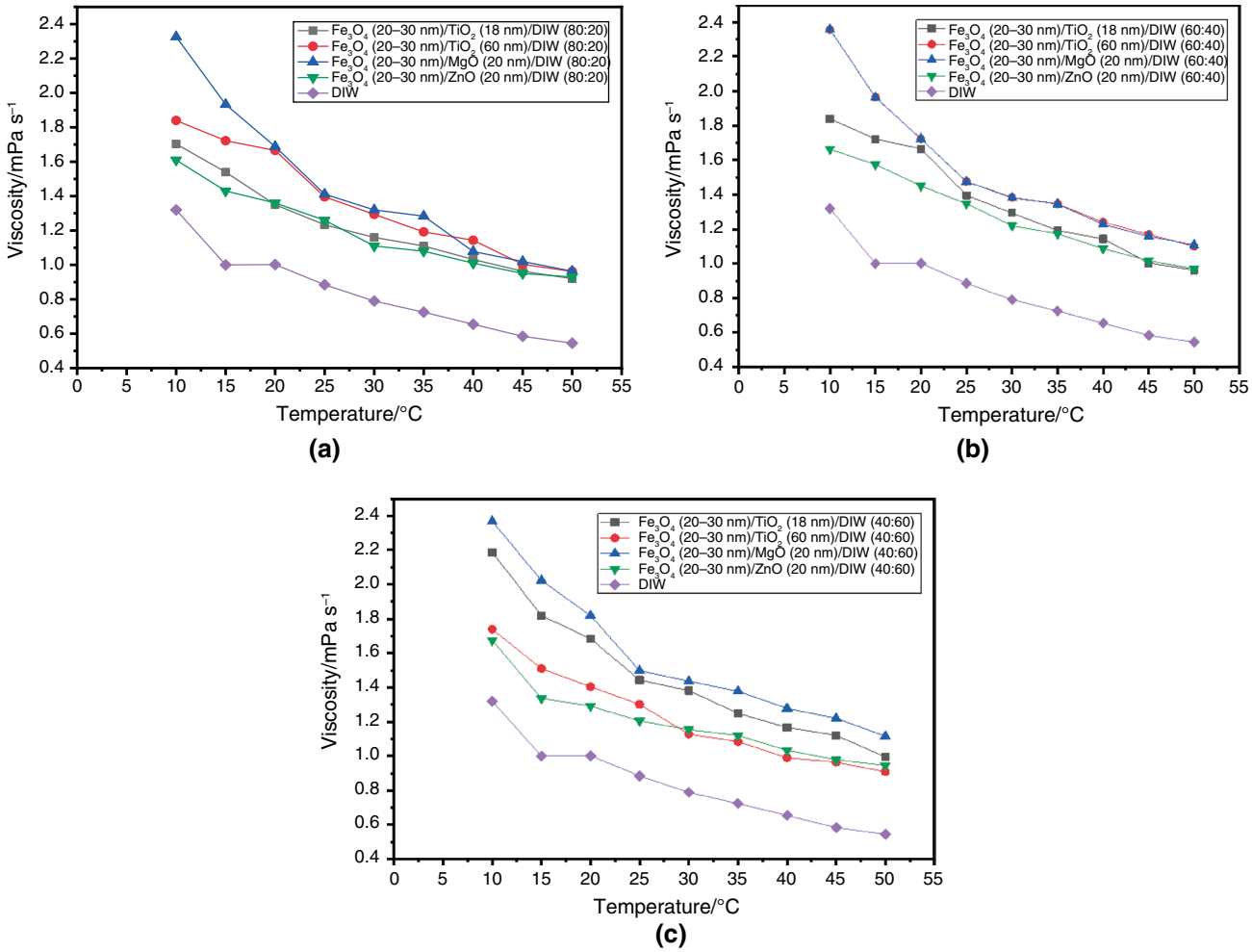

Fig. 13 Viscosities of MHFs/DIW with **a** 80:20, **b** 60:40, and **c** 40:60 at different temperatures

Viscosity model

In this section, machine learning-based linear regression models were developed to correlate the viscosity of DIW and hybrid nanofluids with key parameters such as temperature and nanoparticle composition. Before modeling the hybrid nanofluids, the modeling approach was first validated using DIW to ensure the reliability of the regression methodology. Figure 14 presents the validation of the model with the experimentally measured viscosity in this study and those reported in the studies by Popiel and Wojtkowiak [49] and Yunus and Çengel [50]. The results show a strong agreement between the linear regression model, measured viscosity, and the existing literature studies, with only slight deviations at temperature less than 20 °C.

Subsequently models were developed for hybrid ferrofluids composed of Fe_3O_4 combined with TiO_2, MgO, and ZnO nanoparticles, and their predictive performances were rigorously evaluated using cross-validation and comparison against experimental data in this study and previous

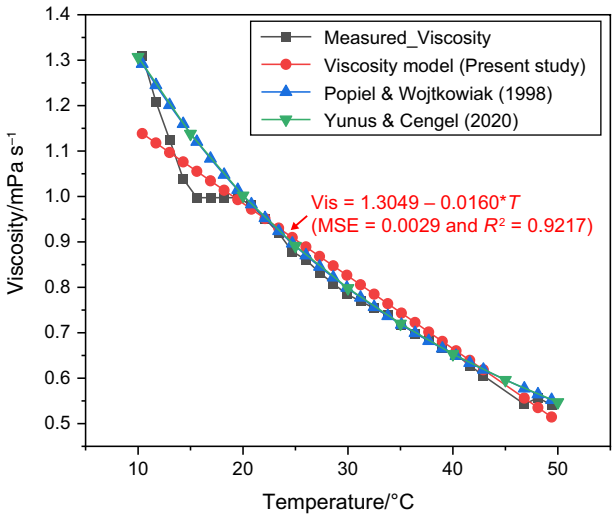

Fig. 14 Validation of viscosity model with experimental results and previous studies

Table 4 Viscosity correlations for hybrid ferrofluids and their performance metrics

Fluid	Viscosity correlation	MSE	R^2/%	CV R^2/ %	CV MSE	CV MAE
DIW	Vis = -0.0160*T + 1.3049	0.0029	92.17	89.69	0.0032	0.0386
Fe_3O_4–TiO_2 (18 nm)/DIW	Vis = − 0.227*T − 0.2474*Fe + 0.2474*Ti + 2.0757	0.00054	94.38	93.21	0.0063	0.0594
Fe_3O_4–TiO_2 (60 nm)/DIW	Vis = − 0.242*T − 0.1674*Fe + 0.1674*Ti + 2.0575	0.02274	80.17	75.85	0.0257	0.1227
Fe_3O_4–MgO/DIW	Vis = − 0.0299*T − 0.1454*Fe + 0.1454*Mg + 2.4322	0.01465	90.66	86.47	0.0170	0.1069
Fe_3O_4–ZnO/DIW	Vis = − 0.0167*T − 0.0006*Fe + 0.0006*Zn + 1.7220	0.00465	90.56	89.03	0.00496	0.0591

literature as summarized in Table 4. The baseline linear regression model developed for DIW demonstrated strong predictive accuracy, achieving an R^2 of 92.17% and a mean squared error (MSE) of 0.0029, with a cross-validated R^2 of 89.69%. Extending the modeling approach to hybrid ferrofluids, the Fe_3O_4-TiO_2 (18 nm)/DIW, the model exhibited the highest predictive performance, with an R^2 of 94.38%, MSE of 0.000536, and a cross-validated (CV) R^2 of 93.21%. The Fe_3O_4-ZnO/DIW and Fe_3O_4-MgO/DIW models also demonstrated high predictive accuracy, yielding R^2 values of 90.56% and 90.66%, and cross-validated R^2 values of 89.03% and 86.47%, respectively. The Fe_3O_4-TiO_2 (60 nm)/DIW model achieved a lower R^2 of 80.17% and a cross-validated R^2 of 75.85%, indicating reduced model generalization.

The regression plots (Fig. 15) further revealed that most data points closely aligned within the 45-degree line, particularly for Fe_3O_4–TiO_2/DIW (18 nm) and Fe_3O_4–ZnO/DIW hybrids, indicating excellent model accuracy. Minor deviations observed for the Fe_3O_4–TiO_2 (60 nm) model, where the cross-validated R^2 dropped to 75.85%, suggested slight limitations in capturing nonlinear effects at larger

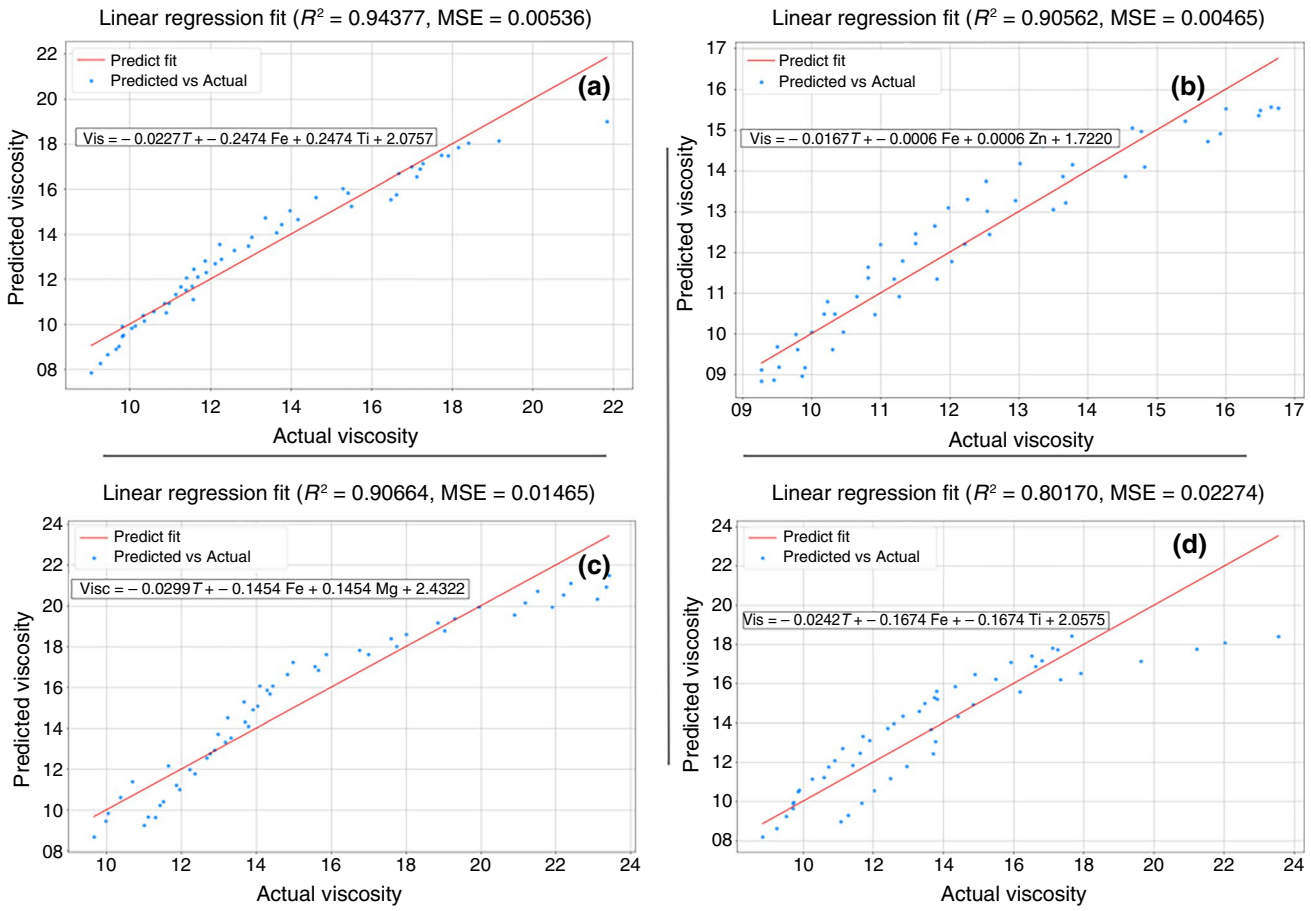

Fig. 15 Linear regression model predictions for viscosity (K) of **a** Fe_3O_4-TiO_2 (18 nm), **b** Fe_3O_4-ZnO, **c** Fe_3O_4-MgO, and **d** Fe_3O_4–TiO_2 (60 nm) DIW hybrid ferrofluids

nanoparticle sizes. Nevertheless, the overall low mean absolute errors (MAEs) and mean squared errors (MSEs) across all hybrid nanofluids affirmed that the developed viscosity models were robust, well-generalized, and reliable for practical prediction across varying temperature and composition ranges.

Influence of temperature on the thermoelectrical conductivity of the MHFs

Based on the viscosity, thermal conductivity, and stability of the fluids examined in the study, we can consider the MHFs with HMR of 80:20 to be the most suitable for heat transfer applications [51], such as cooling in PEM fuel cells and other industrial and energy devices [52]. Therefore, we examine the influence of temperature on the thermoelectrical conductivity of the MHF with an 80:20 HMR, as shown in Fig. 16. The results show that TEC was inversely related to temperature.

The result revealed that Fe_3O_4/ZnO-DIW MHFs have the highest TEC value of 7.86 cm/mS at 10 °C and 4.56 cm/mS at 50 °C, followed by Fe_3O_4/TiO_2(60nm)-DIW, which has a TEC of 5.50 cm/mS at 10 °C and 3.5 cm/mS at 50 °C. Fe_3O_4/TiO_2(18nm)-DIW has the least TEC, with a value of 2.48 cm/mS at 10 °C and 1.6 cm/mS at 50 °C.

These remarkable thermoelectrical conductivity values position all the MHFs considered in this work as a promising choice for maintaining efficient electrical and thermal performance in PEM fuel cell systems, especially for cooling the stacks. Beyond their potential use in cooling proton exchange membrane (PEM) fuel cells, these MHFs show significant promise in several other industrial and technological domains:

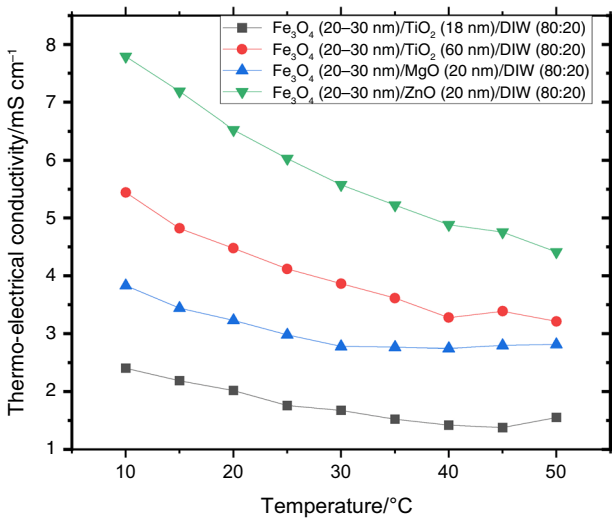

Fig. 16 The impact of temperature on the MHFs TEC

- Electronics and Microelectronics Cooling: The enhanced thermal conductivity and magnetically controllable nature of MHFs make them suitable for the high-performance cooling of CPUs, GPUs, and other densely packed microelectronic components, where efficient thermal dissipation is essential to maintain operational stability [53].
- Automotive and Aerospace Systems: MHFs can serve as next-generation coolants in electric and hybrid vehicle radiators, battery thermal management systems, and regenerative braking units. In aerospace applications, their low density and high heat transfer capability make them attractive for compact, mass-sensitive systems.
- Biomedical and Drug Delivery Applications: The inclusion of Fe_3O_4 in these ferrofluids provides magnetic responsiveness, enabling their use in targeted drug delivery, MRI contrast enhancement, and magnetic hyperthermia for cancer treatment. Hybridization with TiO_2 or ZnO enhances their biocompatibility and stability.
- Solar Thermal Collectors: Due to their strong solar absorption and thermal response, MHFs can be utilized in direct absorption solar collectors, contributing to improved solar-to-thermal energy conversion efficiencies.
- Electrical Equipment Cooling: MHFs are being considered as replacements for conventional transformer oils and dielectric fluids, providing superior heat transfer capabilities and the ability to respond to magnetic fields for enhanced performance control [54].
- Lubrication and Tribological Systems: The rheological adaptability of MHFs under magnetic influence makes them effective as smart lubricants in mechanical systems, improving load-carrying capacity and reducing wear under dynamic operating conditions.

These diverse application areas highlight the technological relevance and multifunctional potential of MHFs, particularly those with optimized mixing ratios, in addressing the evolving thermal management challenges across industries.

Environmental and economic impacts of hybrid ferrofluids in thermal systems

While the incorporation of nanoparticles into base fluids significantly enhances thermophysical performance, a responsible assessment of their environmental and economic impacts is essential for sustainable adoption in thermal and energy systems [55]. The Fe_3O_4-based hybrid ferrofluids investigated in this study, namely Fe_3O_4/TiO_2, Fe_3O_4/MgO, and Fe_3O_4/ZnO dispersed in DIW, offer notable advantages in terms of environmental compatibility and energy efficiency. The selected metal oxides are generally considered among the safer classes of nanomaterials: Fe_3O_4 exhibits

low toxicity and biodegradability, TiO_2 and ZnO are widely used in commercial and industrial products, and MgO is characterized by relatively low environmental and biological risk [56].

From an energy system perspective, the improved thermal conductivity and stability of these hybrid nanofluids support enhanced heat transfer efficiency, enabling better thermal regulation in heat exchangers, cooling loops, and other process systems where they can serve as heat transfer fluids [57]. The magnetic properties of Fe_3O_4 further facilitate active flow control or magnetic field-assisted heat transfer techniques [58]. When applied in industrial-scale systems, these properties contribute to reductions in pumping power, downsizing of heat exchange surfaces, and overall energy savings, leading to long-term operational cost benefits.

Economically, although the initial costs of nanoparticle synthesis and dispersion may be higher than conventional fluids, these are offset by improved energy utilization, reduced equipment size, wear, and potential for performance optimization in high-efficiency applications. Furthermore, magnetic recovery and recycling of Fe_3O_4-based nanoparticles reduce material losses and enable partial circularity in usage cycles [59]. However, concerns remain regarding environmental persistence, aquatic toxicity (particularly for ZnO), and the potential for reactive oxygen species (ROS) formation under UV exposure (notably in TiO_2) [60, 61]. These risks highlight the importance of lifecycle considerations and regulatory compliance in deployment.

To mitigate adverse impacts, the use of eco-friendly surfactants such as the biodegradable gum arabic and the implementation of closed-loop, containment-based system designs are recommended [62]. Incorporating magnetic separation technologies can support nanoparticle recovery, while life cycle assessment (LCA) approaches can quantify environmental trade-offs. For environmentally sensitive or open-loop systems, hybrid nanofluids incorporating MgO or Fe_3O_4 may be prioritized due to their comparatively lower ecological risk profiles. Ultimately, the responsible development and integration of Fe_3O_4-based hybrid ferrofluids into energy systems can yield significant gains in thermal performance, energy efficiency, and environmental sustainability.

Conclusions

This study conducted an experimental investigation into the influence of temperature, hybridization mixing ratio (HMR), and nanoparticle types on the stability, thermal conductivity, viscosity, and TEC of Fe_3O_4/TiO_2(18 nm)-DIW, Fe_3O_4/TiO_2(60 nm)-DIW, Fe_3O_4/MgO-DIW, and Fe_3O_4/ZnO-DIW magnetic hybrid nanofluids (MHFs). The results provide comprehensive insights into the thermophysical properties of MHFs concerning temperature, hybridization mixing ratio, and time. It was found that MHFs with an HMR of 80:20 consistently exhibited superior stability and thermal conductivity, particularly when combined with TiO_2 nanoparticles. Key findings include

i. The thermal conductivity and electrical conductivity were proportional to temperature for all the MHFs.
ii. The Fe_3O_4/ZnO-DIW MHF with an HMR of 80:20 demonstrated the highest thermal conductivity among all, registering a value of 0.793 W/m.K and a percentage enhancement of 31.28% compared to deionized water at 50 °C. MHFs with larger TiO_2 particle size Fe_3O_4/TiO_2 (60 nm)-DIW) exhibited better stability and thermal conductivity when compared to smaller particle size hybrid Fe_3O_4/TiO_2(18 nm)-DIW.
iii. Specifically, the Fe_3O_4/TiO_2(18 nm)-DIW MHF with an HMR of 80:20 showed the highest electrical conductivity of all, registering values of 4.23 mS/cm and 972.93% enhancement compared to deionized water at 50°C.
iv. Furthermore, the Fe_3O_4/ZnO-DIW MHF, regardless of HMR, showed the lowest viscosity among all the MHFs. The MHF with an HMR of 80:20 achieved the lowest viscosity values of 1.62 mPa.S at 10 °C and 0.995 mPa.S at 50 °C.
v. The viscosity and TEC were inversely proportional to the temperature for all the MHFs considered.
vi. The outstanding thermoelectrical conductivity values of the MHFs position them for potential use in PEM fuel cell cooling stacks and other industrial applications.
vii. Correlations for predicting the respective thermal conductivity and viscosity of the MHFs were developed using linear regression.
viii. The feature importance analysis revealed that the temperature of the MHFs is the most significant variable influencing its thermal conductivity.
ix. The hybrid ferrofluids have considerable economic and environmental benefit if adequately managed.

This study underscores the significant impact of temperature, hybridization mixing ratios, and the size and type of nanoparticles on the stability and thermophysical behavior of magnetic hybrid nanofluids (MHFs) for heat transfer applications in industrial and energy systems. The experimental results for viscosity and thermal conductivity were found to align closely with previously established correlations in the literature, reinforcing the reliability of the data and the predictive capability of existing models. This agreement also highlights the potential of the selected ferroparticles for specialized thermal applications, where consistency, enhanced performance, and precise modeling are crucial. Future research will focus on refining temperature- and

ferroparticle-dependent models to improve predictive accuracy, which will be valuable for simulation, design optimization, and practical deployment of MHFs in next-generation thermal management systems.

Funding Open access funding provided by University of Pretoria.

References

1. Choi SUS, Eastman JA. Enhancing thermal conductivity of fluids with nanoparticles. ASME Int Mech Eng Fluids Eng Div FED. 1995;8(231):99–105. https://doi.org/10.1021/je60018a001.
2. Giwa SO, Sharifpur M, Ahmadi MH, Meyer JP. Magnetohydrodynamic convection behaviours of nanofluids in non-square enclosures: a comprehensive review. Math Methods Appl Sci. 2020. https://doi.org/10.1002/MMA.6424.
3. Shah K, Choi S-B. The influence of particle size on the rheological properties of plate-like iron particle based magnetorheological fluids. Smart Mater Struct. 2015;24(1):015004. https://doi.org/10.1088/0964-1726/24/1/015004.
4. Doganay S, Alsangur R, Turgut A. Effect of external magnetic field on thermal conductivity and viscosity of magnetic nanofluids: a review. Mater Res Express. 2019;6(11):112003. https://doi.org/10.1088/2053-1591/ab44e9.
5. el Maazouzi A, Masrour R, Jabar A. Thickness-dependent magnetic properties of inverse spinel Fe_3O_4. Phase Transit. 2020;93(7):733–40. https://doi.org/10.1080/01411594.2020.1771563.
6. Agnihotri P, Lad VN. Magnetic nanofluid: synthesis and characterization. Chem Pap. 2020;74(9):3089–100. https://doi.org/10.1007/s11696-020-01138-w.
7. Shahsavar A, Saghafian M, Salimpour MR, Shafii MB. Experimental investigation on laminar forced convective heat transfer of ferrofluid loaded with carbon nanotubes under constant and alternating magnetic fields. Exp Therm Fluid Sci. 2016;76:1–11. https://doi.org/10.1016/j.expthermflusci.2016.03.010.
8. Sundar LS, Abebaw HM, Singh MK, Pereira AMB, Sousa ACM. Experimental heat transfer and friction factor of Fe_3O_4 magnetic nanofluids flow in a tube under laminar flow at high prandtl numbers. Int J Heat Technol. 2020;38(2):301–13. https://doi.org/10.18280/ijht.380204.
9. Kumar A, Subudhi S. Preparation, characteristics, convection and applications of magnetic nanofluids: a review. Heat Mass Transf und Stoffuebertrag. 2018;54(2):241–65. https://doi.org/10.1007/s00231-017-2114-4.
10. Atofarati EO, Mohsen S, Meyer JP. Parametric influences on nanofluid-jet cooling heat transfer. In: Nanofluids preparation, applications and simulation method. Elsevier; 2024. p. 351–98. https://doi.org/10.1016/B978-0-443-13625-2.00014-0.
11. Chakraborty S, Panigrahi PK. Stability of nanofluid: a review. Appl Therm Eng. 2020;174:115259. https://doi.org/10.1016/j.applthermaleng.2020.115259.
12. Nikkhah V, Sarafraz MM, Hormozi F, Peyghambarzadeh SM. Particulate fouling of CuO–water nanofluid at isothermal diffusive condition inside the conventional heat exchanger-experimental and modeling. Exp Therm Fluid Sci. 2015;60:83–95. https://doi.org/10.1016/J.EXPTHERMFLUSCI.2014.08.009.
13. Hamad EM, et al. Review of nanofluids and their biomedical applications. J Nanofluids. 2021;10(4):463–77. https://doi.org/10.1166/JON.2021.1806.
14. Agista MN, Guo K, Zhixin Y. A state-of-the-art review of nanoparticles application in petroleum with a focus on enhanced oil recovery. Appl Sci. 2018;8(6):871. https://doi.org/10.3390/app8060871.
15. Jana S, Salehi-Khojin A, Zhong WH. Enhancement of fluid thermal conductivity by the addition of single and hybrid nano-additives. Thermochim Acta. 2007;462(1–2):45–55. https://doi.org/10.1016/j.tca.2007.06.009.
16. Giwa SO, Sharifpur M, Meyer JP. Experimental study of thermoconvection performance of hybrid nanofluids of Al_2O_3-MWCNT/water in a differentially heated square cavity. Int J Heat Mass Transf. 2020;148:119072. https://doi.org/10.1016/j.ijheatmasstransfer.2019.119072.
17. Chinnasamy V, Ham J, Cho H. Comparative investigation of convective heat transfer and pressure drop characteristics of MWCNT, Fe_3O_4, and MWCNT/Fe_3O_4 nanofluids. Case Stud Therm Eng. 2023;47:103095. https://doi.org/10.1016/j.csite.2023.103095.
18. Sarboolookzadeh Harandi S, Karimipour A, Afrand M, Akbari M, D'Orazio A. An experimental study on thermal conductivity of F-MWCNTs-Fe3O4/EG hybrid nanofluid: effects of temperature and concentration. Int Commun Heat Mass Transf. 2016;76:171–7. https://doi.org/10.1016/j.icheatmasstransfer.2016.05.029.
19. Sundar LS, Venkata Ramana E, Graça MPF, Singh MK, Sousa ACM. Nanodiamond-Fe_3O_4 nanofluids: preparation and measurement of viscosity, electrical and thermal conductivities. Int Commun Heat Mass Transf. 2016;73:62–74. https://doi.org/10.1016/j.icheatmasstransfer.2016.02.013.
20. Mehrali M, et al. Heat transfer and entropy generation analysis of hybrid graphene/Fe_3O_4 ferro-nanofluid flow under the influence of a magnetic field. Powder Technol. 2017;308:149–57. https://doi.org/10.1016/j.powtec.2016.12.024.
21. Acharya N, Mabood F. On the hydrothermal features of radiative Fe_3O_4–graphene hybrid nanofluid flow over a slippery bended surface with heat source/sink. J Therm Anal Calorim. 2021;143(2):1273–89. https://doi.org/10.1007/S10973-020-09850-1/FIGURES/21.
22. Lund LA, Omar Z, Raza J, Khan I. Magnetohydrodynamic flow of Cu–Fe_3O_4/H_2O hybrid nanofluid with effect of viscous dissipation: dual similarity solutions. J Therm Anal Calorim. 2021;143(2):915–27. https://doi.org/10.1007/s10973-020-09602-1.
23. Lee A, Veerakumar C, Cho H. Effect of magnetic field on the forced convective heat transfer of water–ethylene glycol-based Fe_3O_4 and Fe_3O_4–MWCNT nanofluids. Appl Sci. 2021;11(10):4683. https://doi.org/10.3390/app11104683.
24. Giwa SO, Sharifpur M, Ahmadi MH, Sohel Murshed SM, Meyer JP. Experimental investigation on stability, viscosity, and electrical conductivity of water-based hybrid nanofluid of mwcnt-Fe_2O_3. Nanomaterials. 2021;11(1):1–19. https://doi.org/10.3390/nano11010136.
25. Sundar LS, Singh MK, Sousa ACM. Enhanced heat transfer and friction factor of MWCNT-Fe_3O_4/water hybrid nanofluids. Int Commun Heat Mass Transf. 2014;52:73–83. https://doi.org/10.1016/j.icheatmasstransfer.2014.01.012.

26. Shi L, He Y, Yanwei H, Wang X. Thermophysical properties of Fe_3O_4@CNT nanofluid and controllable heat transfer performance under magnetic field. Energy Convers Manag. 2018;177:249–57. https://doi.org/10.1016/j.enconman.2018.09.046.
27. Shahsavar A, Saghafian M, Salimpour MR, Shafii MB. Effect of temperature and concentration on thermal conductivity and viscosity of ferrofluid loaded with carbon nanotubes. Heat Mass Transf Stoffuebertrag. 2016;52(10):2293–301. https://doi.org/10.1007/s00231-015-1743-8.
28. Liu WI, Alsarraf J, Shahsavar A, Rostamzadeh M, Afrand M, Nguyen TK. Impact of oscillating magnetic field on the thermal-conductivity of water-Fe_3O_4 and water-Fe_3O_4/CNT ferro-fluids: experimental study. J Magn Magn Mater. 2019;484(February):258–65. https://doi.org/10.1016/j.jmmm.2019.04.042.
29. Korei Z, Berrahil F, Filali A, Benissaad S, Boulmerka A. Thermo-magnetic convection analysis of magnetite ferrofluid in an arc-shaped lid-driven electronic chamber with partial heating. J Therm Anal Calorim. 2023;148(6):2585–604. https://doi.org/10.1007/s10973-022-11894-4.
30. Baby TT, Ramaprabhu S. Experimental investigation of the thermal transport properties of a carbon nanohybrid dispersed nanofluid. Nanoscale. 2011;3(5):2208–14. https://doi.org/10.1039/c0nr01024c.
31. Riyadi TWB, et al. Nanofluid heat transfer and machine learning: Insightful review of machine learning for nanofluid heat transfer enhancement in porous media and heat exchangers as sustainable and renewable energy solutions. Results Eng. 2024;24:103002. https://doi.org/10.1016/j.rineng.2024.103002.
32. Longo GA, Zilio C, Ceseracciu E, Reggiani M. Application of artificial neural network (ANN) for the prediction of thermal conductivity of oxide-water nanofluids. Nano Energy. 2012;1(2):290–6. https://doi.org/10.1016/j.nanoen.2011.11.007.
33. He W, et al. Using of artificial neural networks (ANNs) to predict the thermal conductivity of zinc oxide-silver (50%–50%)/Water hybrid Newtonian nanofluid. Int Commun Heat Mass Transf. 2020;116:104645. https://doi.org/10.1016/j.icheatmasstransfer.2020.104645.
34. Zhang T, et al. Optimization of thermophysical properties of nanofluids using a hybrid procedure based on machine learning, multi-objective optimization, and multi-criteria decision-making. Chem Eng J. 2024;485:150059. https://doi.org/10.1016/j.cej.2024.150059.
35. Adogbeji VO, Sharifpur M, Meyer JP. Experimental investigation into heat transfer and flow characteristics of magnetic hybrid nanofluid (Fe_3O_4/TiO_2) in turbulent region. Appl Therm Eng. 2025;258:124630. https://doi.org/10.1016/j.applthermaleng.2024.124630.
36. Zakaria I, Azmi WH, Mohamed WANW, Mamat R, Najafi G. Experimental investigation of thermal conductivity and electrical conductivity of Al_2O_3 nanofluid in water—ethylene glycol mixture for proton exchange membrane fuel cell application. Int Commun Heat Mass Transf. 2015;61:61–8. https://doi.org/10.1016/J.ICHEATMASSTRANSFER.2014.12.015.
37. Awe OO, Atofarati EO, Adeyinka MO, Musa AP, Onasanya EO. Assessing the factors affecting building construction collapse casualty using machine learning techniques: a case of Lagos, Nigeria. Int J Constr Manag. 2023. https://doi.org/10.1080/15623599.2023.2222966.
38. Atofarati EO, Sharifpur M, Huan Z, Awe OO, Meyer JP. Experimental and machine learning study on the influence of nanoparticle size and pulsating flow on heat transfer performance in nanofluid-jet impingement cooling. Appl Therm Eng. 2025;258:124631. https://doi.org/10.1016/J.APPLTHERMALENG.2024.124631.
39. Kulkarni DP, Namburu PK, Edbargar H, Das DK. Convective heat transfer and fluid dynamic characteristics of SiO_2—ethylene glycol/water nanofluid. Heat Transf Eng. 2008;29(12):1027–35. https://doi.org/10.1080/01457630802243055.
40. Momin M, Nwaokocha CN, Sharifpur M, Cheraghian G, Meyer JP, El-Rahman MA. Investigation of thermal and electrical properties of ternary composite nanofluids using MgO, ZnO, and MWCNT nanoparticles. Results Phys. 2025. https://doi.org/10.1016/j.rinp.2025.108139.
41. Abareshi M, Goharshadi EK, Mojtaba Zebarjad S, Khandan Fadafan H, Youssefi A. Fabrication, characterization and measurement of thermal conductivity of Fe_3O_4 nanofluids. J Magn Magn Mater. 2010;322(24):3895–901. https://doi.org/10.1016/j.jmmm.2010.08.016.
42. Giwa SO, Momin M, Nwaokocha CN, Sharifpur M, Meyer JP. Influence of nanoparticles size, per cent mass ratio, and temperature on the thermal properties of water-based MgO–ZnO nanofluid: an experimental approach. J Therm Anal Calorim. 2021;143(2):1063–79. https://doi.org/10.1007/s10973-020-09870-x.
43. Heyhat MM, Irannezhad A. Experimental investigation on the competition between enhancement of electrical and thermal conductivities in water-based nanofluids. J Mol Liq. 2018;268:169–75. https://doi.org/10.1016/j.molliq.2018.07.022.
44. Coetzee D, Venkataraman M, Militky J, Petru M. Influence of nanoparticles on thermal and electrical conductivity of composites. Polymers (Basel). 2020. https://doi.org/10.3390/POLYM12040742.
45. Bagheli S, Fadafan HK, Orimi RL, Ghaemi M. Synthesis and experimental investigation of the electrical conductivity of water based magnetite nanofluids. Powder Technol. 2015;274:426–30. https://doi.org/10.1016/j.powtec.2015.01.050.
46. Giwa SO, Sharifpur M, Goodarzi M, Alsulami H, Meyer JP. Influence of base fluid, temperature, and concentration on the thermophysical properties of hybrid nanofluids of alumina–ferrofluid: experimental data, modeling through enhanced ANN, ANFIS, and curve fitting. J Therm Anal Calorim. 2021;143(6):4149–67. https://doi.org/10.1007/s10973-020-09372-w.
47. Adio SA. Experimental investigation and mathematical modelling of thermophysical properties of ethylene glycol and glycerol-based nanofluids. University of Pretoria, 2015.
48. Awais M, et al. Heat transfer and pressure drop performance of nanofluid: a state-of- the-art review. Int J Thermofluids. 2021;9:100065. https://doi.org/10.1016/j.ijft.2021.100065.
49. Popiel CO, Wojtkowiak J. Simple formulas for thermophysical properties of liquid water for heat transfer calculations (from 0 °c to 150 °c). Heat Transf Eng. 1998;19(3):87–101. https://doi.org/10.1080/01457639808939929.
50. Çengel J, Yunus, Ghajar A, Afshin, Heat and mass transfer in SI units: fundamentals and applications, 6th ed. MCGraw Hill, 2020.
51. Adogbeji VO, Sharifpur M, Meyer JP. International Journal of Thermal Sciences experimental investigation of heat transfer, thermal efficiency, pressure drop, and flow characteristics of Fe_3O_4–MgO magnetic hybrid nanofluid in transitional flow regimes. Int J Therm Sci. 2025;209:109515. https://doi.org/10.1016/j.ijthermalsci.2024.109515.
52. Adogbeji VO, Sharifpur M, Meyer JP. Case studies in thermal engineering experimental investigation of heat transfer enhancement, thermal efficiency, and pressure drop in forced convection of magnetic hybrid nanofluid (Fe_3O_4/TiO_2) under varied magnetic field strengths and waveforms. Case Stud Therm Eng. 2024;63:105313. https://doi.org/10.1016/j.csite.2024.105313.
53. Korei Z, Benissaad S, Chamkha AJ, Berrahil F, Filali A. Thermohydraulic and second law analyses during the cooling of an electronic device mounted in an open cavity equipped with magnetic nanofluid, magnetic field inducer, and porous media: a two-phase numerical investigation. Int Commun Heat Mass Transf.

2022;139:106497. https://doi.org/10.1016/j.icheatmasstransfer.2022.106497.
54. Korei Z, Benissaad S, Filali A, Berrahil F. An investigation of entropy and exergy of nanofluid flow in microchannel heat sinks. J Nanofluids. 2023;12(4):1160–72. https://doi.org/10.1166/jon.2023.2006.
55. Atofarati EO, Sharifpur M, Huan Z. Nanofluids for heat transfer enhancement: a holistic analysis of research advances, technological progress and regulations for health and safety. Cogent Eng. 2024. https://doi.org/10.1080/23311916.2024.2434623.
56. Muddin NAI, Badsha MM, Arafath MA, Merican ZMA, Hossain MS. Magnetic chitosan nanoparticles as a potential bio-sorbent for the removal of Cr(VI) from wastewater: synthesis, environmental impact and challenges. Desalin Water Treat. 2024;319:100449. https://doi.org/10.1016/J.DWT.2024.100449.
57. Khalil S, Yasmin H, Abbas T, Muhammad T. Analysis of thermal conductivity variation in magneto-hybrid nanofluids flow through porous medium with variable viscosity and slip boundary. Case Stud Therm Eng. 2024;57:104314. https://doi.org/10.1016/J.CSITE.2024.104314.
58. Adogbeji VO, Atofarati EO, Sharifpur M, Meyer JP. Results in physics magnetohydrodynamics of nanofluid internal forced convection : a review and outlook for practical applications. Results Phys. 2025;68:108082. https://doi.org/10.1016/j.rinp.2024.108082.
59. Li Y, Wang Z, Wang L, Xie H, Hong H, Yu W. Efficient photothermal conversion and recycling of magnetic highly viscous oil-based nanofluids. Appl Therm Eng. 2025;265:125532. https://doi.org/10.1016/J.APPLTHERMALENG.2025.125532.
60. Shohag S, Horie Y. Neurotoxicity and cardiovascular toxicity of zinc oxide nanoparticles to *Oryzias melastigma*. J Appl Toxicol. 2025;45(3):452–9. https://doi.org/10.1002/JAT.4718.
61. Yu C, et al. Generation of reactive oxygen species on MIL-100(Fe)/TiO_2 driven by mild natural light. ChemCatChem. 2024;16(19):e202400847. https://doi.org/10.1002/CCTC.202400847.
62. Patra N. Integrated process for eco-friendly synthesis and coating of ZrB2 onto carbon fiber substrates. Colloids Surf A Physicochem Eng Asp. 2024;703:135310. https://doi.org/10.1016/J.COLSURFA.2024.135310.